Journal of Structural Geology 198 (2025) 105445

Contents lists available at ScienceDirect

Journal of Structural Geology

journal homepage: www.elsevier.com/locate/jsg

Multi-millennia slip rate relationships between closely spaced across-strike faults: Temporal earthquake clustering of the Skinos and Pisia Faults, Greece, from *in situ* ^{36}Cl cosmogenic exposure dating

Sam Mitchell [a,*], Claudia Sgambato [a], Jenni Robertson [a], Gerald P. Roberts [a], Joanna P. Faure Walker [b], Zoë Mildon [c], Athanassios Ganas [d], Ioannis Papanikolaou [e], Francesco Iezzi [f], Joakim Beck [g], Steven A. Binnie [h], Tibor Dunai [h], Damián A. López [h], Georgios Deligiannakis [e], Silke Mechernich [i], Klaus Reicherter [j], Elias J. Rugen [k]

[a] *Department of Natural Sciences, Birkbeck College, University of London, UK*
[b] *Department of Risk and Disaster Reduction, University College London, UK*
[c] *School of Geography, Earth and Environmental Sciences, University of Plymouth, UK*
[d] *Institute of Geodynamics, National Observatory of Athens, Greece*
[e] *Natural Resources and Agricultural Engineering, Agricultural University of Athens, Greece*
[f] *Department of Earth Sciences, Environment and Resources, University of Naples Federico II, Italy*
[g] *Computer, Electrical and Mathematical Sciences and Engineering, King Abdullah University of Science and Technology (KAUST), Saudi Arabia*
[h] *Institute for Geology and Mineralogy, University of Cologne, Germany*
[i] *Formerly at Institute for Geology and Mineralogy, University of Cologne, Germany*
[j] *Institute of Neotectonics and Natural Hazards, RWTH Aachen University, Germany*
[k] *Department of Earth Sciences, University College London, UK*

A R T I C L E I N F O

Keywords:
Across-strike faults
Fault interaction
Temporal clustering
In situ ^{36}Cl cosmogenic dating
Normal faulting earthquakes
Greece

A B S T R A C T

This study investigates slip behaviour on overlapping, *en echelon* normal faults by analysing the slip histories of the Skinos and Pisia active normal faults over the past ~20 kyrs using *in situ* ^{36}Cl cosmogenic dating. New ^{36}Cl data from the Skinos Fault and published Pisia Fault ^{36}Cl data were modelled, with both sample sites located within an overlap zone and separated by an across-strike distance of 1–2 km. Our analysis reveals fluctuating slip rates, with the two faults alternating between out-of-phase and simultaneous slip. The Pisia Fault exhibited a slip rate of ~0.5–0.75 mm/yr from ~20 ka to ~9.6 ka, increasing to ~1.25 mm/yr until ~5.2 ka. It then slowed to ~0.25 mm/yr or less until ~2.0 ka, before accelerating again to ~1.25–1.5 mm/yr to the present day. The Skinos Fault maintained a low slip rate of ~0.25 mm/yr or less from ~20 ka to ~6.4 ka, before accelerating to ~2.0–3.0 mm/yr, persisting to ~1.0 ka or possibly the present-day. Comparing their slip histories, the faults show periods of simultaneous slip between ~6.4 ka to ~5.2 ka and ~2.0 ka to ~1.0–0.0 ka, and out-of-phase slip occurred between ~9.6 ka and ~6.4 ka, and from ~5.2 ka to ~2.0 ka. Out-of-phase behaviour on faults across strike has now been observed on faults spaced across-strike at distances of 1–2 km, 10–20 km, and ~100 km, raising the question of why it occurs. Possible mechanism(s), including rheological fluctuations within fault/shear-zone structures linked between the brittle upper crust and viscous lower crust and stress interactions, are discussed to explain the out-of-phase and simultaneous slip behaviour.

1. Introduction

Understanding the temporal behaviour of active faults is crucial in deciphering the mechanisms that control continental deformation. It is now recognised that slip rates on active faults fluctuate through time, with periods of rapid slip lasting multiple millennia alternating with periods with less rapid slip, or even no slip. The periods of rapid slip are associated with surface displacements that are too large to be produced by a single earthquake slip (e.g. Wells and Coppersmith, 1994; Wesnousky, 2008), suggesting the existence of temporal clusters of surface

* Corresponding author.
E-mail address: sam.mitchell@bbk.ac.uk (S. Mitchell).

https://doi.org/10.1016/j.jsg.2025.105445
Received 10 January 2025; Received in revised form 16 April 2025; Accepted 21 April 2025
Available online 26 April 2025

faulting earthquakes (>Ms 6.0) (Mechernich et al., 2018, 2023; Iezzi et al., 2021; Mildon et al., 2022; Roberts et al., 2024; Dolan et al. 2007, 2024; Dolan and Meade, 2017). Conversely, relatively low slip rate periods indicate temporal earthquake anticlustering, where a lack of large magnitude surface-faulting earthquakes in given time periods produces a slip rate that falls below the background long-term slip rate (e.g. Mechernich et al., 2018; Iezzi et al., 2021; Mildon et al., 2022; Mechernich et al., 2023; Roberts et al., 2024).

It has been shown that the periods of rapid slip associated with the temporal clustering of surface faulting earthquakes can be out-of-phase on faults located across strike from one another (across-strike faults). Such out-of-phase behaviour has been documented on faults spaced 100s of kilometres apart across strike, such as the Los Angeles-region faults and the eastern California shear zone in USA (Dolan et al., 2007; Scholz, 2010), Garlock, San Andreas and Eastern California Shear Zone fault system in USA (Dolan et al., 2016), and North Anatolian, Kunlun and Denali Faults (Dolan and Meade, 2017). The behaviour has also been identified on faults spaced 10s of kilometres across strike, such as the Milesi, Malakasa and Fili Faults in Greece (Iezzi et al., 2021), the Mt. Vettore and Leonessa Faults (Mildon et al., 2022) and the Maiella, Scanno and Pescasseroli Faults in Italy (Roberts et al., 2024), and the Wairau, Awatere, Clarence and Hope Faults in New Zealand (Dolan et al., 2024). Microstructural evolution, including annealing and strain-hardening, and interaction through stress transfer have been invoked to explain such behaviour. However, little is known about whether active across-strike faults spaced only a few kilometres apart exhibit similar out-of-phase slip relationships, and what mechanism(s) might be operating to produce these slip rate fluctuations. This unknown is important because many examples exist where faults spaced only a few kilometres apart have ruptured simultaneously or closely-spaced in time (e.g. the 1915 Pleasant Valley, 1959 Hebgen Lake, 1954 Dixie Valley and Fairview Peak, and 1981 Gulf of Corinth earthquakes; Wallace et al., 1984; Doser, 1985; Slemmons, 1957; Scholz, 2010; Jackson et al., 1982).

For examples spaced 100s of kilometres apart across strike, it has been suggested that out-of-phase slip may be explained by cycles of strain hardening and annealing within shear zones in the middle to lower crust beneath the brittle active faults (Dolan et al., 2007; Dolan and Meade, 2017). An example of such out-of-phase slip at this scale has been identified between the Los Angeles-region faults and the eastern California shear zone (USA), where faults are too far apart to be interacting through static stress transfer (Dolan et al., 2007; Ganas et al., 2006; Papadopoulos et al., 2017). The activation of a temporal earthquake cluster is suggested to occur when annealing of a viscous shear zone, through the introduction of new strain-free grains, weakens the shear zone to an extent that causes deformation to migrate to that location. Strain hardening during slip then develops and increases resistance to deformation through microstructural evolution on the shear zone. Strain hardening continues until deformation migrates to a shear-zone across strike that has become annealed, initiating a temporal cluster of surface faulting earthquakes in that new location (Dolan et al., 2007; Dolan and Meade, 2017). Thus, the across-strike shear-zones have differing microstructural histories.

For examples spaced 10s of kilometres apart across strike, it has been suggested that out-of-phase slip may be explained by fault interactions where slip induces differential stress changes on neighbouring across-strike fault/shear-zones which result in the switching between periods of temporal clustering and anticlustering (Mildon et al., 2022; Roberts et al., 2024). Examples of this have been reported for active normal faults in the central Apennines, Italy (Mildon et al., 2022; Roberts et al., 2024). It is suggested that fluctuations in differential stress on shear-zones during interaction induce changes in viscous strain rate, quantified by flow laws linking stress and strain-rate (e.g. Hirth et al., 2001). These changes in viscous strain-rate at depth on shear-zones then produce changes in the slip rates on overlying brittle faults. Mildon et al. (2022) and Roberts et al. (2024) showed that the magnitudes of differential stress changes calculated for periods of increased and decreased slip rate were sufficient to explain observed fluctuations in slip rates constrained with *in situ* ^{36}Cl cosmogenic dating on fault planes. Thus, the across-strike shear-zones have differing stress transfer histories.

However, for examples of faults spaced only a few kilometres apart, it is likely that they share the same underlying shear-zone, because envisaged shear-zone thicknesses of a few kilometres at most are similar to across strike fault spacing (Moore and Parsons, 2015; Cowie et al., 2013; Fossen and Cavalcante, 2017). This may imply that it is unlikely that individual faults have differing annealing, strain-hardening or differential stress histories for viscous deformation at depth. Thus, the question arises as to whether such closely-spaced faults show out-of-phase behaviour, prompting this study.

In this study, we investigate slip relationships between two active normal faults spaced only 1–2 km across strike in central Greece, the Skinos and Pisia Faults, which ruptured within hours of each other during the 1981 eastern Gulf of Corinth earthquake sequence (Ms 6.7 and Ms 6.4) (Fig. 1). To achieve this, we (1) reconstruct the slip rate histories of both faults over the last ~20 kyr using *in situ* ^{36}Cl cosmogenic exposure dating, (2) examine their temporal slip relationships, revealing alternating periods of high and low slip rates as well as both out-of-phase and simultaneous slip relationships, and (3) explore the mechanisms driving these interactions and their implications for seismic hazard. By understanding the slip behaviour of closely spaced faults, this study provides critical insights into single and multi-fault earthquake scenarios through identifying periods in which one fault ruptures or periods in which both across-strike faults rupture simultaneously or closely spaced in time. These findings are essential for improving seismic hazard assessments in regions with complex fault networks, particularly where closely spaced faults may interact and potentially trigger multiple earthquakes.

2. Background

2.1. Geological background

Extension in Greece occurs in crust thickened by Alpine thrusting alongside slab-roll back of the north-dipping Hellenic subduction zone between the African and Eurasian Plates (Jolivet et al., 1994; Jolivet, 2001) and dextral motion of the North Anatolian strike-slip Fault (Kelletat et al., 1976; Le Pichon and Angelier, 1979; Westaway, 1991; Jackson, 1994; Jolivet et al., 1994, 2013; Le Pichon et al., 1995). This tectonic setting is associated with extension throughout Greece for the past ~5 million years, predominantly in a north-south orientation, resulting in the formation of normal faults (Billiris et al., 1991; Jackson, 1994; Armijo et al., 1996; Clarke et al., 1998; Roberts and Ganas, 2000; Goldsworthy et al., 2002; Vassilakis et al., 2011). Extension in the Corinth rift is accommodated by normal faults predominantly striking ~E-W and producing extension in a N-S direction (e.g. McKenzie, 1972; Taymaz et al., 1991; Billiris et al., 1991; Jackson, 1994; Roberts and Ganas, 2000; Bell et al., 2009; Nixon et al., 2016; Evelpidou et al., 2023). GNSS-derived extension rates in the eastern region of the gulf, the region we study, indicate a rate of 5–6 mm/yr, contrasting with a higher rate of 10–11 mm/yr in the western region (see Briole et al., 2021, their Fig. 7 for the regional GNSS vectors) (Fig. 1a). The footwalls of the normal faults consist predominantly of Mesozoic limestones, with Neogene sediments found in some areas, along with rare outcrops of ultrabasic ophiolitic rocks and deep-sea cherts in places (Roberts and Jackson, 1991; Papanikolaou, 2009, 2013; Walker et al., 2010; Ford et al., 2013; Whittaker and Walker, 2015). The hanging walls are occupied by sediments formed from the erosion of footwall rocks, consisting of Neogene-Holocene fluvio-terrestrial sediments, including alluvium, colluvium and marine deposits at coastal sites (Roberts and Jackson, 1991; Goldsworthy and Jackson, 2000; Leeder et al., 2005; Rohais et al., 2007; Sakellariou et al., 2007; Taylor et al., 2011; Ford et al., 2013;

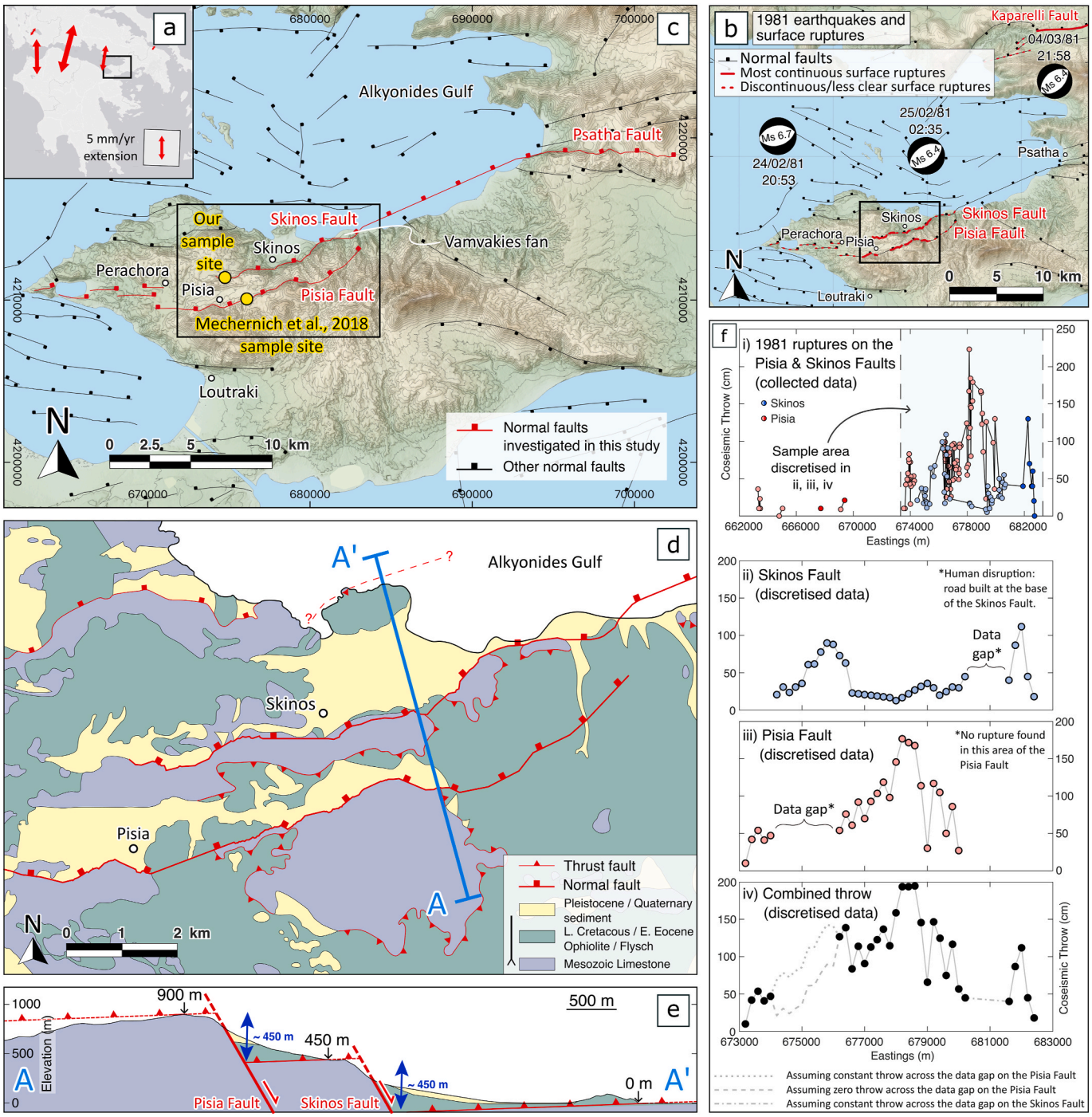

Fig. 1. Details of the Pisia and Skinos Faults. (a) Coastline map of mainland Greece with extension rates from Briole et al. (2021) and the location of area (c) in the black box. (b) Map of the 1981 surface ruptures (red solid) on the Pisia, Skinos and Kaparelli Faults (Jackson et al., 1982; Mitchell et al., 2024) and the location of the ruptures in (f.ii,iii,iv) in the black box. Focal mechanisms are displayed at the inferred epicentres of the three earthquakes of the 1981 eastern Gulf of Corinth earthquake sequence (Hubert et al., 1996). (c) Map of the Perachora Peninsula and the eastern Gulf of Corinth region with surface traces of normal faults (Ganas et al., 2013; Mitchell et al., 2024) showing the entire South Alkyonides Fault System (Pisia, Skinos and Psatha Faults) and the location of area (d) in the black box. The locations of the ^{36}Cl sample sites are shown in yellow. The Skinos Fault sample site is located at 674762 m E, 4211384 m N (lat 38.033325°, long 22.991320°) and the Pisia Fault sample site (Mechernich et al., 2018) is located at 676105 m E, 4210067 m N (lat 38.021202°, long 23.006291°). (d) Geological map of the area of overlap between the across-strike Skinos and Pisia Faults with a cross-section line for (e) oriented NNW-SSE using map sheets (1:50,000) Kaparellion and Perahora (IGME Kaparellion Geological Map Bornovas et al., 1984; IGME Perachora Geological Map Bornovas et al., 1984). (e) Cross-section through the Pisia and Skinos Faults showing the offset of a thrust of ~450 m each (lithology key is the same as in (d)). (f) Comparing the 1981 coseismic throw profiles on the Pisia and Skinos Faults (data sourced from Mitchell et al., 2024 with additional measurements from Collier et al., 1998; Roberts and Ganas, 2000). (i) Field measured coseismic throw data from the Perachora Peninsula to Vamvakies Fan. Pale and dark blue circles are Skinos Fault data recorded by Mitchell et al. (2024) and Collier et al. (1998) respectively. Pale and dark red circles are Pisia Fault data recorded by Mitchell et al. (2024) and Roberts and Ganas (2000) respectively. Solid line connects data of ruptures on each fault. In (ii) and (iii) the throw profiles of the Skinos and Pisia Faults are discretised from the data in (i), respectively. (iv) Combined discretised data by summing the throw values from (ii) and (iii). Coordinate system: WGS 84/UTM Zone 34 S. (For interpretation of the references to colour in this figure legend, the reader is referred to the Web version of this article.)

Papanikolaou et al., 2015; Gawthorpe et al., 2018; Gawthorpe et al., 2022).

Seismicity in central Greece and the Peloponnese due to normal faulting is widespread, with examples known from as far back as at least 464 BC, documented by the ancient Greek philosopher Plutarch who reported a devastating earthquake in the Sparta region (Guidoboni et al., 1994). More recent historical records have shown frequent, moderate-to-large destructive earthquakes (<~Ms 6.7; Ambraseys and Jackson, 1990). The most recent and well documented destructive earthquakes in the eastern Gulf of Corinth region were in February–March 1981 (Fig. 1b).

During the 1981 eastern Gulf of Corinth earthquake sequence, slip on the Pisia, Skinos and Kaparelli normal faults was associated with surface rupturing during three earthquakes on the 24th and 25th February, and 4th March with Ms = 6.7, 6.4 and 6.4, respectively, causing 22 fatalities (Fig. 1b) (Jackson et al., 1982; Vita-Finzi and King, 1985; Stewart and Hancock, 1991). Following detailed analyses of the surface ruptures and seismicity produced by the 1981 earthquakes, the 24th and February 25, 1981 earthquakes were attributed to the Pisia and Skinos Faults (Jackson et al., 1982; Taymaz et al., 1991; Abercrombie et al., 1995; Mitchell et al., 2024). The approximately 25 km long Pisia Fault is arranged in a left-stepping, across-strike and *en echelon* geometry relative to the approximately 30 km long Skinos Fault, which is likely connected along strike to the Psatha Fault (Jackson et al., 1982). The Pisia, Skinos and Psatha Faults are considered to be part of the ~40 km-long South Alkyonides Fault System (Roberts, 1996; Morewood and Roberts, 1997, 1999, 2001; Morewood and Roberts, 1997; Roberts et al., 2009) (Fig. 1c). In the zone of overlap, the Pisia and Skinos Faults are separated by less than 1–2 km across-strike, with both faults displacing a thrust sheet containing ophiolite by ~450 m each (Fig. 1d and e). At depth, the geometry and arrangement of the faults are unknown, and it is unclear if the faults link at depth (Roberts, 1996; Mitchell et al., 2024). Along-strike to the east from this fault system, the 4th March earthquake occurred on the south-dipping Kaparelli Fault (Fig. 1b). For the Pisia and Skinos Faults, determining which ruptures were associated with each of the earthquakes is challenging, because both earthquakes occurred within hours of each other overnight, at 20:53 and 02:35 local time (Jackson et al., 1982). The ruptures were mapped in the days and weeks after the earthquakes (Jackson et al., 1982; IGME Kaparellion Geological Map Bornovas et al., 1984; IGME Perachora Geological Map Bornovas et al., 1984). Ruptures on the Pisia and Skinos Faults were partially re-mapped in 1994 and 1995 (Roberts, 1996), and then mapped in more detail in 2022, revealing semi-continuous surface ruptures that extended ~8–10 km on each fault within the *en echelon* zone of overlap (Fig. 1fi) (Mitchell et al., 2024). The ruptures produced a single maximum asymmetric profile on the Pisia Fault with a maximum coseismic throw of 223 cm, and a double maxima profile on the Skinos Fault with a maximum throw of 109 cm and 130 cm (Mitchell et al., 2024). Comparing the two sets of ruptures across-strike revealed that the faults were spatially anticorrelated which implies interaction between the faults, because coseismic slip deficits on one fault are compensated by slip maxima on the other fault, and vice versa (Fig. 1fii,iii) (Mitchell et al., 2024). Summing the two throw profiles from the 1981 ruptures across strike in the zone of overlap revealed a single maximum symmetric bell-like profile (combined discretised maximum displacement of ~2 m) implying that the two faults worked together during the 1981 earthquake sequence (Fig. 1fiv) (Mitchell et al., 2024). However, examination of earlier ruptures preserved as a 2nd lichen stripe higher on the exhumed fault planes show that the along strike displacement profiles differed in previous earthquakes on the two faults implying non-characteristic earthquakes (Mitchell et al., 2024; see also Roberts, 1996).

Although no other along-strike profiles for previous ruptures exist for the Skinos and Pisia Faults, paleoseismological analysis of the two faults has revealed multiple earthquakes on both faults during the Holocene (Collier et al., 1998; Mechernich et al., 2018). Cosmogenic ^{36}Cl exposure analysis of a carbonate fault scarp on the Pisia Fault suggests the occurrence of six to eight moderate to large paleoearthquakes during the Holocene with more slip back to ~30 ka (Mechernich et al., 2018). Modelling by Mechernich et al. (2018) revealed an average slip rate of 0.5–0.6 mm/yr over the last ~7.3 kyrs, and a period of higher slip rate of up to 0.8–2.3 mm/yr between ~7 and 10 ka. It is worth noting that the sampled scarp of the Pisia Fault in Mechernich et al. (2018) began to form earlier than the widely accepted view for the timing of the demise of the high erosion rates that characterised the Last Glacial Maximum (LGM) at 15 ± 3 ka (Giraudi and Frezzotti, 1986, 1997; Allen et al., 1999; Palumbo et al., 2004). Since scarp preservation could only begin once erosion rates no longer exceeded fault slip rates, the scarp age of ~30 ka being older than the age of the end of the high erosion rates suggests that regional variations influenced the timing of the end of the high erosion rates. For example, Iezzi et al. (2021) suggested that differences in latitude and elevation may have caused the colder, high erosion rate conditions of the LGM to cease earlier at some fault scarp sites, allowing scarp formation and preservation to commence sooner. The slip rate variations determined by Mechernich et al. (2018) on the Pisia Fault have been verified by mapping elevations of radiocarbon-dated Holocene coastal notches which were deformed along the strike of the fault associated with earthquake clusters and quiescence implied by *in situ* ^{36}Cl on the Pisia Fault (Robertson et al., in review). For the Skinos Fault, palaeoseismic trenching and associated radiocarbon ages on ruptured sediments of the Vamvakies fan, also known as Bambakies fan, situated on the Skinos Fault (e.g. Collier et al., 1998) suggest up to six previous paleoearthquakes which were comparable to the displacements produced during the 1981 earthquakes (Collier et al., 1998). An average throw rate was calculated to be 0.7–2.5 mm/yr on the Skinos Fault over the last ~1.5 kyrs with a suggested earthquake recurrence of 330 years (Collier et al., 1998). However, this paleoseismic record for the Skinos Fault is less complete or absent prior to 6–8 ka, or possibly as far back as 12.4 ka, due to the Vamvakies fan only forming when rising Holocene sea level achieved its current elevation, thus no earthquakes prior to this are likely to be recorded in its stratigraphy (Fairbanks, 1989; Leeder et al., 1991; Collier et al., 1998; Peckover et al., 2019). This highlights the need for a record of slip on the Skinos Fault that can be compared with that of the Pisia Fault whose record stretches back possibly as far as 30 ka (Mechernich et al., 2018), prompting this study.

2.2. *In situ* ^{36}Cl cosmogenic exposure dating of limestone fault scarps

Measuring ^{36}Cl concentrations can help us understand the slip history of a fault because, after the demise of high erosion rates associated with the LGM, fault scarps began to accumulate and preserve ^{36}Cl through interactions between calcium atoms and cosmic radiation. As a result, higher concentrations of ^{36}Cl are found at the top of exposed fault planes within fault scarps because the higher parts have been exposed for a longer duration (Benedetti et al., 2002, 2003; Schlagenhauf et al., 2010) (illustrated in Fig. 2a and b). ^{36}Cl begins to form in carbonate at depths of up to 10 m or more beneath the surface due to exposure interactions between the carbonates at depth and incoming muons (Fig. 2c) (Zreda et al., 1991; Davis and Schaeffer, 1955; Stone et al., 1998; Zreda and Noller, 1998; Gosse and Phillips, 2001; Dunai, 2010). However, overall the rate of production of ^{36}Cl increases towards the surface where the spallation of calcium atoms due to interactions with incoming neutrons becomes the dominant ^{36}Cl production process (Gosse and Phillips, 2001; Schlagenhauf et al., 2010). In general, below a depth of 2 m, the rate of production is below ~5 at(atoms)/g/yr due to shielding by, for example, surrounding bedrock and colluvium (Stone et al., 1996; Schlagenhauf et al., 2010). Again, in general, at the surface, the ^{36}Cl production rate in limestone is ~48 at/g/yr (e.g. Schlagenhauf et al., 2010), but varies with elevation and latitude (Stone et al., 1998; Dunai, 2010). The values stated above are approximate and more detailed production rate scenarios need to be calculated for individual

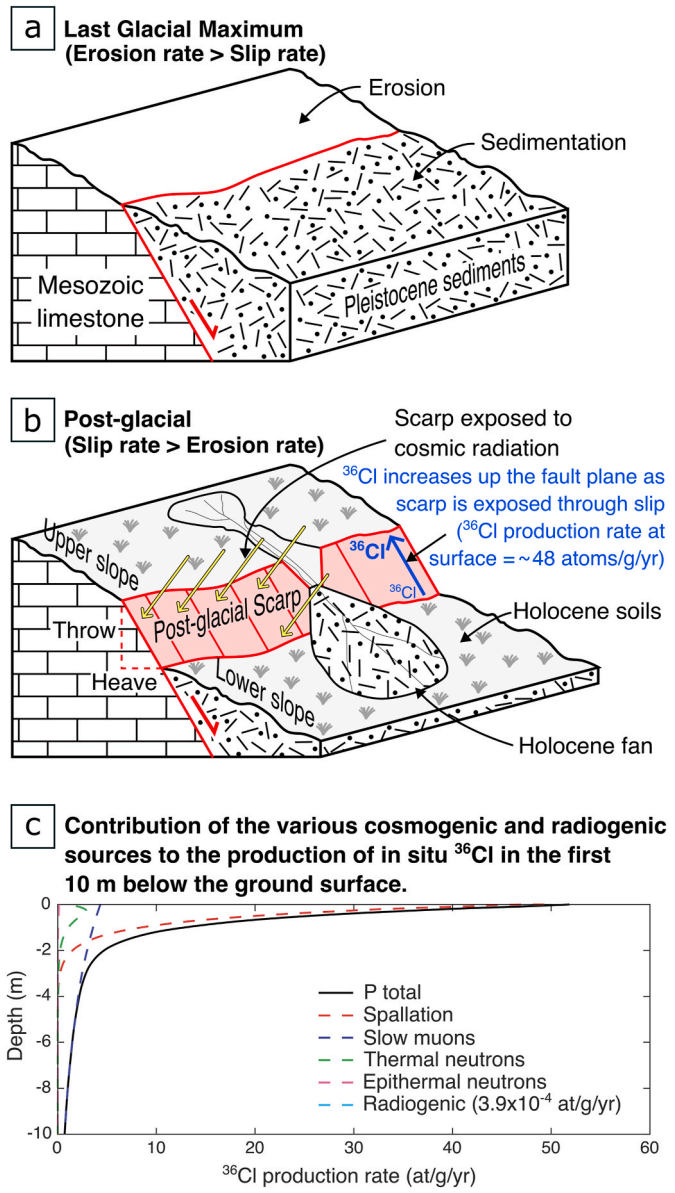

Fig. 2. Evolution of post-glacial scarps and the production of ^{36}Cl on fault planes due to exposure through slip. Illustration (a) demonstrates no fault scarp preservation above the surface during the last glacial maximum (adapted from Roberts and Michetti, 2004); (b) demonstrates fault scarp preservation above the surface during/after the demise of the last glacial maximum (adapted from Roberts and Michetti, 2004). Graph (c) shows the contribution of the various cosmogenic and radiogenic sources to the production of *in situ* ^{36}Cl in the first 10 m below the ground surface (modified from Schlagenhauf et al., 2010).

sites using knowledge of production scaling with latitude and elevation produced by global and temporal variations in the Earth's magnetic field and local atmospheric thickness above mountainous topography (Lal, 1991; Stone, 2000; Dunai, 2000). One way to deal with uncertainties in the above in the absence of measured cosmogenic production rates is to iterate the production values during modelling, for example, as implemented in the code by Beck et al. (2018). The modelling attempts to replicate the measured ^{36}Cl derived from Accelerator Mass Spectrometry and attempts to constrain the exhumation history of the rock samples as they were exhumed up through the sub-surface ^{36}Cl production zone. Additional considerations include the site shielding due to topographic slopes, rock densities, the elemental composition of the rock targets and the colluvium through which some cosmic radiation passes, variations in the geomagnetic field over time, assumptions about production rates with depth (as shown in Fig. 2c), and other parameters, along with the inherent uncertainty associated with all these factors. The model results must then be interpreted by considering quantitative results such as the least squares solution for the comparison between the measured and modelled ^{36}Cl concentrations, the ensemble of top least squares solutions, and the posterior distribution of highest likelihood solutions. Aspects of such modelling are explained in the next section.

We note that while ^{36}Cl dating is valuable for identifying changes in slip rates on faults over multiple millennia (e.g. Palumbo et al., 2004; Schlagenhauf et al., 2011; Benedetti et al., 2013; Tesson et al., 2016; Pousse-Beltran et al., 2022), there are a range of other methods available for analysing fault activity, such as paleoseismic trenching (e.g. Galli et al., 2008; Galli et al., 2022) and U-Pb dating of fault zone cements (e.g. Curzi et al., 2021). However, the advantage of ^{36}Cl cosmogenic exposure dating of limestone fault scarps is that it provides temporal coverage lasting 10s of millennia with the resolution of timing of slip of ±0.5 kyrs (Beck et al., 2018).

3. Methods

We sampled the carbonate Skinos fault plane for *in situ* ^{36}Cl cosmogenic dating to provide a dataset that can be compared with the dataset for the Pisia Fault, sampled by Mechernich et al. (2018) (Fig. 3). The Skinos Fault site was selected because, like the Pisia site, it lies within the zone of overlap between the two faults and is situated less than 2 km from the Pisia Fault site (Fig. 1c). The exact site was ultimately chosen based on exhibiting the distinct geomorphic characteristics of a tectonically exhumed fault scarp, as required for a^{36}Cl sample site (Cowie et al., 2017). These observations include confirming that the scarp offsets a slope that has not been affected by erosion or sedimentation. In detail, this means that we do not sample unless it can be confirmed that there are no incised gullies in the immediate footwall or the hanging wall, the lower slope to fault plane contact is horizontal and not prone to along-strike mass wasting, and no landsliding is present in the immediate vicinity of the sample sites. These observations confirm the scarp was exposed through surface faulting, rather than erosion/sedimentation or mass wasting.

As per other previous examples (e.g. Iezzi et al., 2021; Mildon et al., 2022), we collected multiple samples up the free face in the orientation of the fault slip vector, with sample spacing of 23–40 cm and greater towards the top of the fault, with 50 and 60 cm spacing for the two highest samples (Fig. 3aii). We also excavated an ~80 cm deep trench and sampled the carbonate fault plane in the sub-surface. Site characteristics used to model the ^{36}Cl data are shown in Fig. 3 and tabulated in Electronic Supplement S1a. The magnetic field scaling parameters for the sample site, determined using Stone et al. (1996), and based on latitude and altitude, are provided in Electronic Supplement S1b. Sample preparation and measurement procedures on Cologne AMS, and including the relevant major and trace element chemistries of the samples are given in Electronic Supplement S1c alongside elemental data from ICP-OES. The composition of the colluvium used in our study is derived from the average chemical composition of colluvium samples collected in central Italy that have similar provenance (Cowie et al., 2017). The Italian Apennines have comparable climate conditions and parental Mesozoic carbonate rocks and volcanic inputs with those found in central Greece.

Following previous papers (Iezzi et al., 2021; Mildon et al., 2022; Mechernich et al., 2023; Roberts et al., 2024, 2025; Sgambato et al., 2025), we utilised the Beck et al. (2018) code to model the slip history of the Skinos Fault and re-model the slip history of the Pisia Fault. This code is designed to recover slip rate variations on faults from continuous or discontinuous sampling. The code is provided with the site characteristics and knowledge and uncertainties associated with ^{36}Cl production, and proposes fault slip histories, calculates the implied ^{36}Cl profiles for the proposed slip histories, and compares these with the measured ^{36}Cl concentrations using a Bayesian Markov Chain Monte Carlo

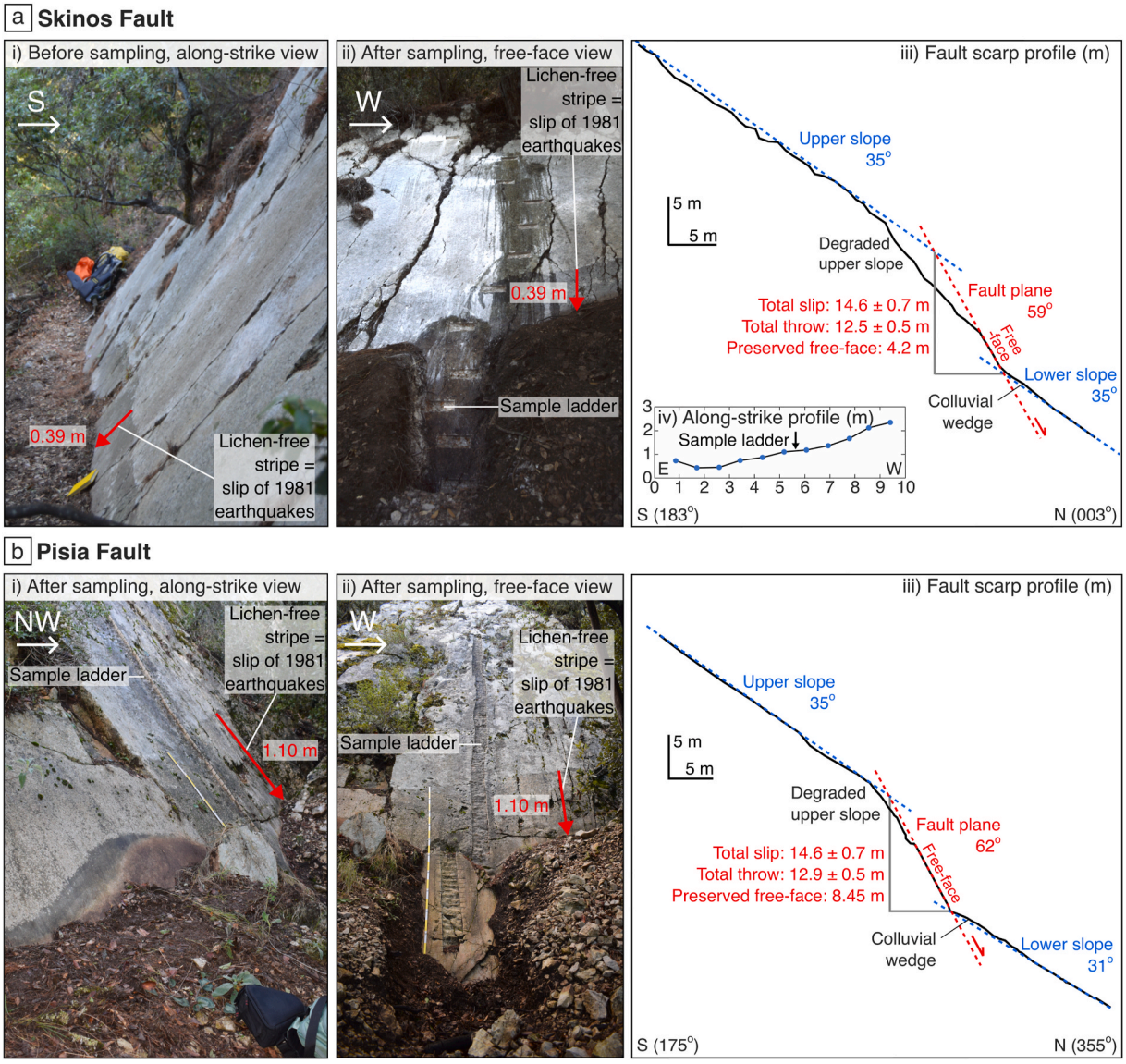

Fig. 3. ^{36}Cl sample sites and fault scarp field measurements on the (a) Skinos Fault and (b) Pisia Fault (see Mechernich et al., 2018, their sample site P6). (a.i,b.i) Limestone fault plane site photographs of (a) the Skinos Fault before sampling, and of (b) the Pisia Fault after sampling with an along-strike view. (a.ii,b.ii) Site photographs of the sample ladder on the fault planes and clear lichen-free stripes of the 1981 earthquake rupture with the view facing the free-face. (a.iii,b.iii) Topographic scarp profiles parallel to the slip vectors recorded in (a) the study herein and (b) Mechernich et al. (2018). (a.iv) Along-strike profile of the hanging wall cut-off. Note the preserved freeface is larger at the Pisia site than the Skinos site.

(MCMC) approach (Beck et al., 2018). The code operates iteratively, conducting simulations of slip histories hundreds of thousands to millions of times. The reader should bear in mind that ^{36}Cl production factors are not precisely known, so we chose to use the Beck et al. (2018) code in order to iterate these values rather than selecting single values (compare with Schlagenhauf et al., 2010; Tikhomirov et al., 2019; Tesson and Benedetti, 2019). The code iterates colluvial density, production rates, and attenuation lengths associated with spallation and muonogenic ^{36}Cl production and displays the results as histograms from the posterior distributions (Fig. 6). The code accounts for uncertainties in input parameters and model set-up, and tests for convergence onto a stable result using two parallel Markov chains (see Beck et al., 2018 for more details). Unlike methods which predefine the number of slip events and displacement sizes (e.g. Schlagenhauf et al., 2010; Tikhomirov et al., 2019; Tesson and Benedetti, 2019), the Beck et al. (2018) code iteratively searches for these parameters. The iterative approach facilitates identification of periods of high or low slip rates, potentially associated with temporal earthquake clustering, rather than individual earthquakes. Additionally, proposed slip histories are drawn from a Brownian-passage-time model (BPT) of earthquake recurrence over a time period set by the user. We have chosen 120 ka for the start of the model runs, with the code choosing the time when erosion rates decreased associated with the demise of the last glaciation through iteration of this value guided by the fit of predicted ^{36}Cl concentrations to measured ^{36}Cl concentrations. The BPT model allows the possibility of both constant and fluctuating pre-LGM slip rates to generate possible ^{36}Cl concentrations from this time, rather than using a single value for pre-exposure or glacial period slip rate (see Schlagenhauf et al., 2010; Tesson and Benedetti, 2019). The modelling ranks slip-histories using the fit of proposed ^{36}Cl concentrations to the measured values, using the least squares solution, an ensemble of the top 1000 least squares solutions (or another number of choice), and the posterior distribution of highest likelihood solutions, showing the median and 90 % confidence bands after a 50 % model run burn-in. Full model results for the two sites are presented in Electronic Supplement S2ab and S2bb. The age of the fault scarp is not required to be pre-defined in the Beck et al. (2018) code

and we do not force the code to constrain the slip history to be only after the LGM because it has been shown that the age of different fault scarps likely vary based on factors such as elevation and latitude (Iezzi et al., 2021).

Once the two parallel Markov chains in the Beck code have converged, as quantified using the Gelman-Rubin test (see Electronic Supplement S2ab and S2bb), we then interpret the initiation and termination of each cluster or anticluster from model output (compare Figs. 4 and 5). These interpretations are based on the consideration of three indicators from the modelled ^{36}Cl slip history (e.g. see Roberts et al., 2024). Increases (cluster initiation) and decreases (cluster termination) in slip rate are identified using the following: (1) steepening and shallowing staircase patterns in the least squares solution, which offers the best fit to the data; (2) concave-up and concave-down inflections in the 90 % confidence lines derived from the full posterior distribution; (3) the density of models derived from, for example, the top 10000, 2000 and/or top 100 least squares solutions, to be chosen by the user. The interpretation of the duration of a period of clustering or anticlustering and the amount of slip in a cluster is therefore somewhat subjective due to the possible bias of the user, but we argue that clear signals of fluctuating slip rate can be identified within the results, accepting a likely ~ ±0.5 kyrs of uncertainty associated with the timing of our interpretations.

Also, we only interpret periods of rapid slip as earthquake clusters where the slip accumulated is too large to be accommodated by single earthquakes (Iezzi et al., 2021), defined by the maximum expected coseismic slip for a given fault as per length-displacement scaling (Wells and Coppersmith, 1994). Anticlusters are periods of relatively low to no slip between clusters, and these periods have slip rates that are lower than that defined by the total slip since slip was preserved, as defined by the modelling of the ^{36}Cl data. It is challenging to calculate the exact slip rates implied by our modelling because of the subjective choice of how to weight the (1) least squares slip history, (2) the ensemble of least squares slip histories or (3) the median slip history from the posterior distribution. To address this, we used a combination of all three statistical solutions to aid our interpretations of the slip rates through time. To aid visualization of the results, we show representative gradients of different slip-rates as part of the key in Fig. 4aii, bii, and 5ai, bi. The slip rate uncertainty we assign of ±0.5 mm/yr was constrained by iterative adjustments of pixel dimensions in the least squares models during visualization. Since pixel size is a subjective choice, the uncertainties themselves are subjective.

4. Results

4.1. Field site characteristics of the Skinos Fault

The ^{36}Cl sampling site on the Skinos Fault was chosen from the structural mapping of the fault zone and 1981 ruptures conducted by Mitchell et al. (2024); their site 324. The key field measured parameters used for modelling include a fault dip of 59°, a post-glacial slip of 14.6 m, a trench depth of 0.73 m, and lower and upper slope dips of 35°.

The chosen site meets the ^{36}Cl sample site selection criteria of Cowie et al. (2017), confirming that the scarp was exhumed by surface faulting rather than sedimentation, erosion, and post-depositional disturbance. The chosen site exhibits the following attributes: (1) The hanging wall cut-off is horizontal and un-incised, lacking sediment cones, which rules out burial by sediment supply from the footwall; (2) the fault plane forms a sub-horizontal contact with the lower slope, so this excludes localised mass movement both perpendicular to the fault and along strike; (3) the lower slope is free of incised gullies, so this excludes the possibility of erosion or sedimentation contributing to exhumation or

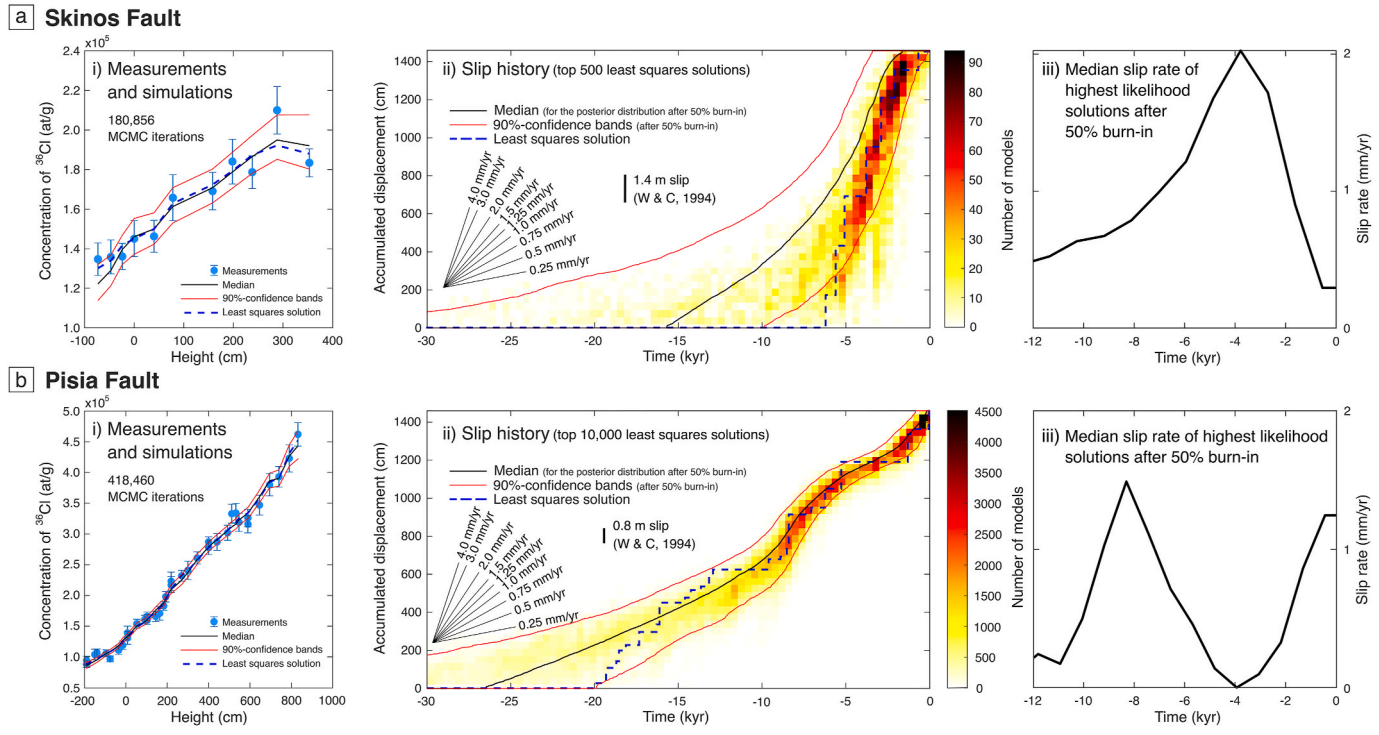

Fig. 4. Measured ^{36}Cl concentrations and slip histories recovered by modelling for the (a) Skinos Fault (^{36}Cl concentrations from our study) and (b) Pisia Fault (^{36}Cl concentrations from Mechernich et al., 2018 and remodelled herein). (a.i,b.i) Measured ^{36}Cl concentrations versus distance in the plane of the fault for the samples extracted at the sites in Fig. 3 with the modelled replications of the data from MCMC modelling of the ^{36}Cl data. (a.ii,b.ii) Slip histories recovered from the modelling. The word "top" refers to the solutions which minimise the sum of the squares of the residuals between measured and modelled ^{36}Cl concentrations. (a.iii,b.iii) Median slip rates for the same model runs as (a.ii) and (b.ii) after 50 % burn-in. The median slip rate is calculated by size of slip events multiplied by their frequency divided by bin size for all model runs in the posterior distribution and bin size is defined as the optimal bin size for the distributions. See Beck et al. (2018) and Roberts et al. (2024) for more details of the modelling procedure and methods for displaying results.

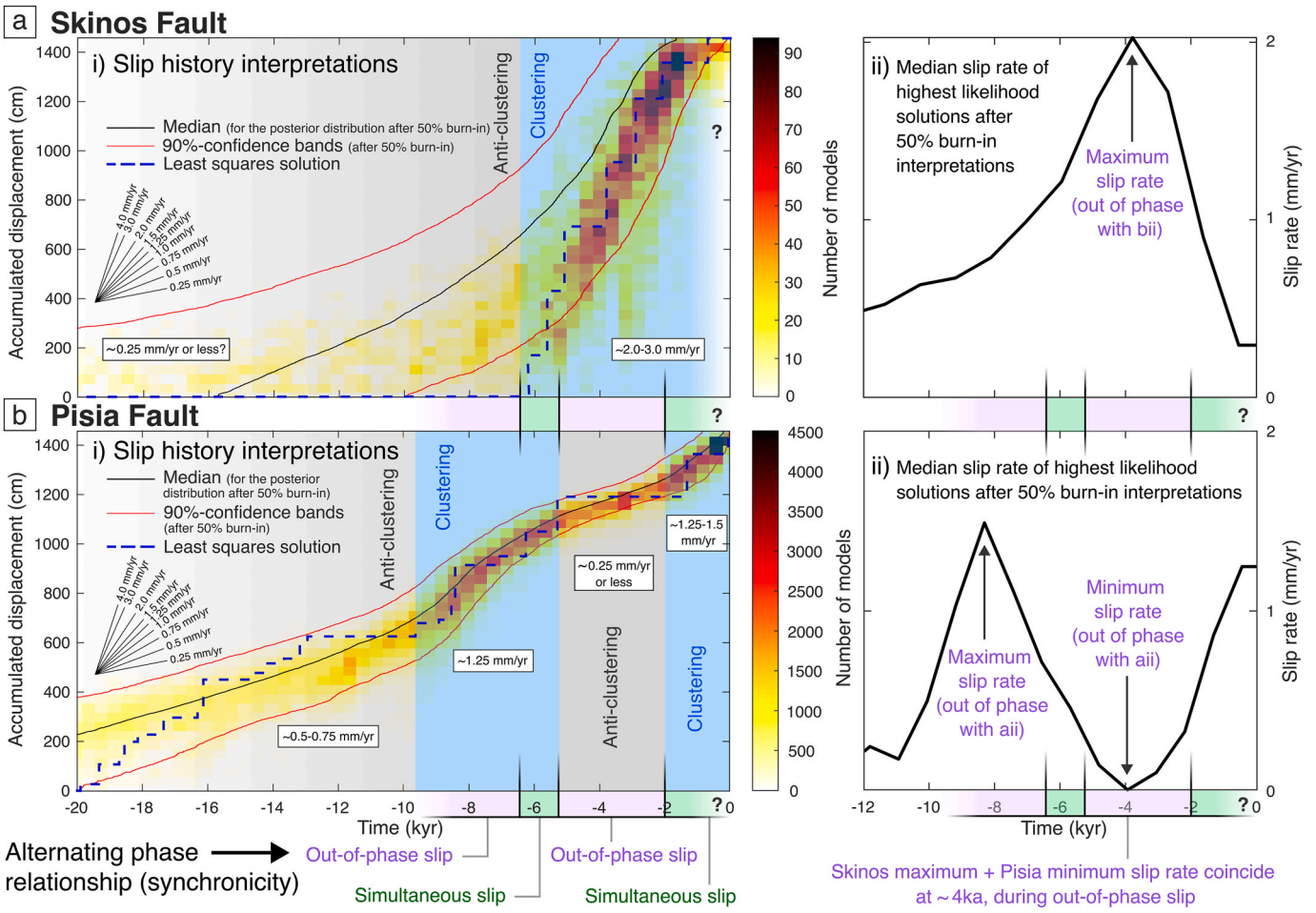

Fig. 5. Interpretations of slip histories for the (a) Skinos Fault and (b) Pisia Fault. (a.i,b.i) Slip in the planes of the faults indicated by the least squares solutions, the ensemble of least squares solutions and the posterior distribution derived from MCMC modelling of the ^{36}Cl data. The interpreted slip rates in white boxes are averaged within each period. Blue rectangles show periods of high slip rate (temporal cluster). Grey rectangles show periods of relatively low slip rate (temporal anticluster). Purple rectangles indicate periods when one fault is experiencing a high slip rate while the other is in a low slip rate. Green rectangles indicate periods when both faults are experiencing relatively high slip rates. (a.ii,b.ii) Out-of-phase slip behaviour indicated by the median slip rate of highest likelihood solutions derived solely from the posterior distribution after 50 % model burn-in for the same model runs as (a.i) and (b.i). (For interpretation of the references to colour in this figure legend, the reader is referred to the Web version of this article.)

burial through time; and (4) similarly, the upper slope is preserved and planar with no incised gullies so as to exclude movement of material from the footwall to the hanging wall after scarp formation. These characteristics confirm that fault plane exposure resulted from surface faulting after slope stabilisation, with slope stabilisation occurring due to the reduction of free-thaw action associated with the climatic conditions associated with the LGM (Piccardi et al., 1999; Roberts and Michetti, 2004; Cowie et al., 2017; Iezzi et al., 2021; Mildon et al., 2022) (Fig. 2a and b and Fig. 3aiv).

4.2. ^{36}Cl concentrations of the Skinos Fault

The concentrations of ^{36}Cl increase up the dip and slip vector azimuth of the fault planes and this is due to more ^{36}Cl being formed through longer exposure up the fault scarp as the fault slips (Fig. 4ai,bi). Disturbances in this trend can be produced by variations in the Ca concentrations, as well as changes in slip rates. However, we measure the Ca concentration for each sample and the code is provided with this information. The concentration profiles differ for the Pisia and Skinos sites with the highest measured values at the Pisia site reaching 4.75 × 10^5 at/g, whereas the topmost samples from the Skinos site exhibit lower concentrations of 2.1 × 10^5 at/g. This is due to a combination of the different extents of the preserved and hence sampled fault planes, but also due to differing exposure histories and we show the results of modelling in Fig. 4aii and 4bii and our temporal cluster interpretations in Fig. 5ai and 5bi. Note that we did encounter one anomalously low ^{36}Cl measurement at +118 m on the Skinos Fault (see Electronic Supplement S1c). Examination of this sample showed that the anomalously low ^{36}Cl in this sample is coincident with local fractures. It is likely that the local fractures contain low ^{36}Cl because fractures are pathways for the influx of meteoric water which might precipitate a young calcite vadose cement (mineral precipitate from infiltrating water in the unsaturated zone above the water table). This would lead to lower overall ^{36}Cl concentration in the overall bulk sample. As this sample was probably altered in its ^{36}Cl concentration by non-tectonic causes, we excluded it from the modelling.

4.3. ^{36}Cl modelling results and slip rate interpretations

The results of the MCMC modelling, shown in Figs. 4 and 5, reveal fluctuations in slip rate through time and Fig. 6 shows the parameters that were iterated during the modelling. The results show that surface slip has progressively produced growth of the fault scarps. Slip rates on both faults were variable over multiple millennia and some constraints have been resolved on the timing of when slip started to be preserved, that is, the age of the preserved scarp (Figs. 4 and 5). Surface slip has

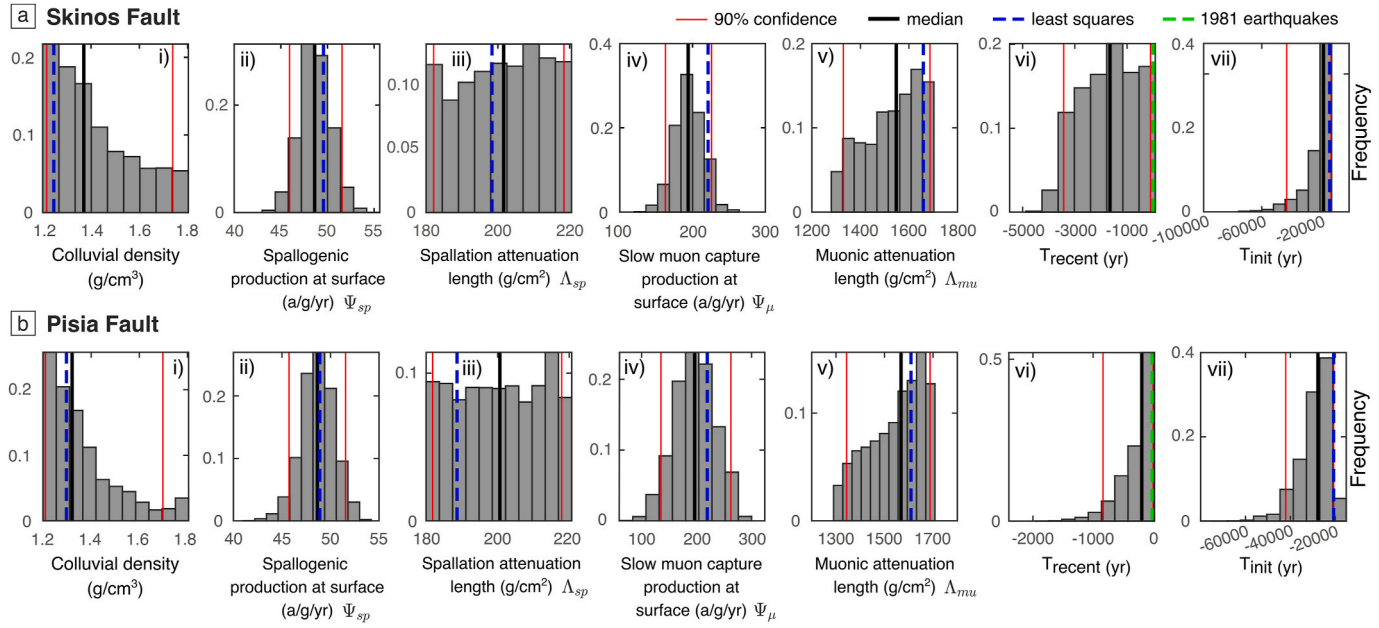

Fig. 6. Parameters iterated in the MCMC modelling of the ^{36}Cl data on the (a) Skinos Fault and (b) Pisia Fault. Medians and 90 % confidence from the posterior distributions after 50 % burn-in for (i) colluvial density, (ii) spallogenic production, (iii) spallation attenuation length, (iv) slow muon capture, (v) muonic attenuation length, (vi) age of last earthquake (Trecent) and (vii) age from which production is preserved (Tinit), and the values for the least squares solution. The 1981 earthquakes are indicated on (vi).

been preserved since at least ~20 ka (see Electronic Supplement S2af and S2bf) but the certainty of older slip history is limited by the availability of preserved fault plane exposures. The upper part of the fault plane was eroded, so no sampling was possible of its earliest exposed surfaces, as indicated by the measured scarp profiles (Fig. 3aiii, biii). The Skinos Fault site has a preserved free-face of only 4.2 m, compared to 8.45 m at the Pisia site, which may contribute to the less clear early slip history on the Skinos Fault. However, the older part of the slip history is also constrained to a degree by the overall shape of the ^{36}Cl profile and hence the exhumation history of the younger samples. Thus, in Figs. 4 and 5 we mainly concentrated our interpretations on the younger parts of the slip histories which are likely to be better constrained. In addition, while the Pisia samples were extracted with closely-spaced samples, and the Skinos samples were less closely spaced, this and previous studies (see Electronic Supplement S2c and Iezzi et al., 2021, their supplementary material S3c) show that degrading the number of samples up to a point does not affect the overall slip history, confirming the robustness and reliability of the results.

The slip rate histories inferred from ^{36}Cl modelling suggest that the two faults have experienced different alternating periods of rapid slip and little or no slip over the last ~20 ka (Fig. 5ai,bi). Based on the modelled results, we interpret that the Pisia Fault had a low slip rate of ~0.5–0.75 mm/yr from ~20 ka to 9.6 ± 0.5 ka, which was followed by a relatively high slip rate of ~1.25 mm/yr from 9.6 ± 0.5 ka to 5.2 ± 0.5 ka (Fig. 5bi). At 5.2 ± 0.5 ka, the Pisia Fault slows to a low slip rate of ~0.25 mm/yr or less, maintaining this relatively low slip rate until 2.0 ± 0.5 ka. Subsequently, from 2.0 ± 0.5 ka to the present day, the slip rate on the Pisia Fault sees an increase to ~1.25–1.5 mm/yr from its previously lower slip rate. Regarding the Skinos Fault, we observe a very low slip rate of ~0.25 mm/yr or less from ~20 ka to 6.4 ± 0.5 ka (Fig. 5ai). At 6.4 ± 0.5 ka to the present day or possibly around ~1.0 ± 0.5 ka, the Skinos Fault accelerates to a very high slip rate of ~2.0–3.0 mm/yr. These values on the Skinos Fault are consistent with throw rate estimates from a paleoseismic trenching site located 8 km along the strike of the Skinos Fault on the Vamvakies fan (0.7–2.5 mm/yr over the last ~1.5 kyrs; Collier et al., 1998), which closely align with the throw rate derived in this study (~1.7–2.6 mm/yr over the same period, converted from a slip rate of ~2.0–3.0 mm/yr and a fault dip of 59°).

A notable observation we make from comparing the slip rate histories of the two faults is that, at times, specifically from ~9.4 ka to ~6.4 ka and ~5.2 ka to ~2.0 ka, their patterns of alternating periods of slip are out-of-phase with each other; one fault has high slip rates whilst the other fault has low slip rates and vice versa (Fig. 5). This out-of-phase relationship seems to dominate and is especially clear in the pattern of slip rates displayed by the median of the posterior distribution of highest likelihood solutions (Fig. 5aii,bii) at ~4.0 ka as the Skinos Fault had a maximum slip rate of ~2 mm/yr whilst the Pisia Fault had a minimum slip rate of near 0 mm/yr. At other times, we observe periods of simultaneous slip of the two faults, for example from 6.4 ± 0.5 ka to 5.2 ± 0.5 ka and 2.0 ± 0.5 ka to the present day or possibly ~1.0 ± 0.5 ka (Fig. 5ai,bi); both faults have relatively high slip rates at the same time. During the first instance of simultaneous slip, the Pisia Fault seems to be slowing down whilst the Skinos Fault seems to accelerate. Conversely, during the second instance of simultaneous slip from 2.0 ± 0.5 ka to possibly the present day whereby the Skinos Fault appears to be slowing, whilst the Pisia Fault appears to be accelerating. Overall, these results suggest a long-term alternation between periods of out-of-phase slip and periods of simultaneous slip, and during the latter, their slip rates switch in opposite directions, with the faults exhibiting either acceleration or deceleration.

Note the exact values for slip rate in Fig. 5aii and 5bii are challenging to interpret because this figure only shows the results from the posterior distribution which will include results from immediately after reverse jumps in the Markov chains, so the exact values are difficult to extract but generally the pattern shows that the faults are out-of-phase at ~4.0 ka.

The slip rate patterns can also be visualised with regard to best fit between the measured and modelled ^{36}Cl concentrations using the least squares solutions and ensembles of least squares solutions (Figs. 4 and 5).

5. Discussion

Our overall finding is that sampled parts of the Pisia and Skinos

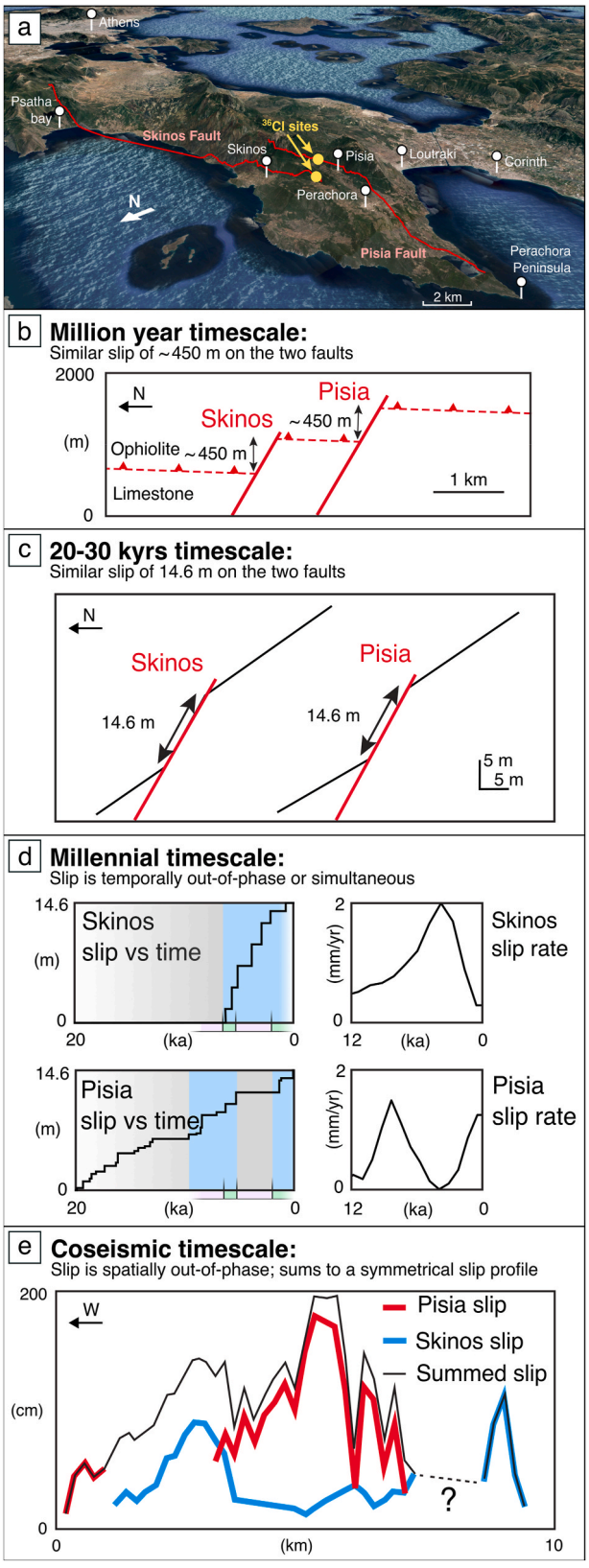

(caption on next page)

Fig. 7. Summary of slip relationships between the Skinos and Pisia Faults. (a) 3D tectonic map of the Perachora peninsula showing the Pisia and Skinos Fault traces and locations of the ^{36}Cl sample sites from our study and Mechernich et al. (2018). (b) Schematic cross-section across the Gerania Mountains simplified from Fig. 1d showing the two north-dipping faults producing two half grabens with both faults displacing a thrust-derived ophiolite fragment by ~450 m each and the displacements that we presently observe likely developed over the million(s) years timescale. (c) Schematic scarp profiles of the Pisia and Skinos Faults simplified from Fig. 3aiii and 3biii showing both faults have 14.6 m of post-glacial slip each over 20–30 kyrs. (d) Slip rate histories and slip rate changes of the Skinos and Pisia Faults simplified from Fig. 5 showing the changes in slip rate on both faults and their out of phase and simultaneous slip relationships. Blue rectangles show periods of high slip rate (temporal cluster). Grey rectangles show periods of relatively slow slip rate (temporal anticluster). Purple rectangles indicate periods when one fault is experiencing a high slip rate while the other is in a low slip rate. Green rectangles indicate periods when both faults are experiencing relatively high slip rates (same as Fig. 5). Only the least squares solutions are displayed on the slip vs time plots. (e) The discretised coseismic throw profiles from the 1981 earthquakes on the Pisia and Skinos Faults in the zone of overlap between the faults simplified from Fig. 1fii-iv showing the anti-correlated relationship of the along-strike throw profiles between the Pisia and Skinos Faults and the combined throw profile displaying a symmetrical shape (Mitchell et al., 2024). (For interpretation of the references to colour in this figure legend, the reader is referred to the Web version of this article.)

Faults show temporal periods of alternating out-of-phase or simultaneous slip on a multi-millennial timescale. This alternating slip behaviour through time exists alongside knowledge that both faults (a) ruptured in the 1981 earthquake sequence with spatially out-of-phase slip (Fig. 1f; Mitchell et al., 2024), (b) share very similar total offsets of Alpine thrust sheets that developed on the millions of years timescale (Fig. 1e), (c) share similar offsets across post-demise of the LGM faults scarps that developed over the last few tens of millennia (Fig. 3aiii and 3biii), and (d) share the same regional stress and velocity fields (Fig. 1; Billiris et al., 1991; Briole et al., 2021) (Fig. 7). The close proximity of the two faults, which form an *en echelon* arrangement with an along-strike overlap of ~8–10 km and an across-strike spacing of 1–2 km (Fig. 1), together with spatially out-of-phase slip on the timescale of a single earthquake sequence and the temporally out-of-phase slip over multiple millennia, suggest interactions between the two fault structures. Below we discuss the possible reasons for this complex fault behaviour.

We have documented, periods of temporally out-of-phase slip on the Skinos and Pisia Faults, and, as mentioned above, this phenomenon has been reported by other authors (e.g. Dolan et al., 2007; Iezzi et al., 2021; Mildon et al., 2022; Roberts et al., 2024). However, unlike other examples whereby the across-strike faults are likely to have separate shear zones at depth due to across-strike distances of 100 s km (Fig. 8a; e.g. Dolan et al., 2007) or 10 s km (Fig. 8b; e.g. Mildon et al., 2022; Roberts et al., 2024) between the faults, the proximity of the closely spaced (less than 1–2 km of across-strike separation) Skinos and Pisia Faults implies that it is unlikely that they have separate shear zones. Thus, it is unlikely that the out-of-phase slip on the Skinos and Pisia Faults can be explained by different overall conditions for their shear zones, such as annealing versus strain-hardening (Dolan et al., 2007) or differential stress changes inducing changes in strain rate (Mildon et al., 2022; Roberts et al., 2024); another mechanism(s) must be at work to produce the out-of-phase slip (Fig. 8c).

We suggest that the out-of-phase slip relationship and periods of simultaneous slip on both faults imply that the faults are working together as one on a millennial timescale, so that the overall slip rate is shared between the faults to accommodate the regional strain rate. Both faults can slip at the same time, perhaps with slip dispersed through an anastomosing network of brittle faults above the brittle-viscous transition which connects the Skinos and Pisia Faults (Fig. 8cii-vi). In other words, at times it appears that the slip rate on the underlying shear-zone makes its way upwards through the interconnected anastomosing network of brittle faults at the brittle-viscous transition, and eventually separates upwards onto the discrete Skinos and Pisia Faults (Fig. 8civ, vii). At other times, the faults slip separately, perhaps because slip through an anastomosing network targets the weaker fault, causing the weaker fault to slip without the other fault slipping (Fig. 8cii,iii,v,vi). Contrasts in strength could be caused by, for example, heterogeneities in the fault gouges in the upper crust or perhaps even fluid involvement. If there is low frictional resistance on both faults due to the gouge having undergone strain-softening during its microstructural evolution, both faults may slip during the same time period. Alternatively, if there is relatively high frictional resistance due to strain-hardening of one fault's gouge, the other fault might slip. Changes in the frictional resistance in gouges may result from microscale processes such as crystallographic orientation changes, grain-size variations, or fluid content changes (e.g. Cladouhos, 1999; Roberts et al., 1993; Ohl et al., 2021; Angevine et al., 1982; Di Toro et al., 2011; Zhu et al., 2020), or the influence of rate and state friction (Biemiller and Lavier, 2017). While our study does not include microscale analyses, similar frictional processes have been observed on multiple faults in the Corinth Rift including the Skinos Fault. For example, carbonate fault rocks on these faults have been shown to undergo cyclic grain-size reduction and induration phases, and cyclic production of crystallographic preferred orientations leading to grain-boundary migration and annealing, influencing frictional resistance over time (Roberts et al., 1993; Ohl et al., 2021). In other fault zones, grain-size reduction and grain attrition has been suggested to reduce stress concentration at grain-to-grain contacts, which can lead to gouge to lock-up and hence strain-hardening (Cladouhos, 1999). In contrast, introduction of new grains plucked from the damage zone can re-set the grain-size distribution, increasing stresses at grain boundaries, which can lead to strain-softening (Cladouhos, 1999). Additionally, the introduction of fluids can either lubricate the slip by reducing normal stresses (e.g. Di Toro et al., 2011; Zhu et al., 2020) or promote cementation or diffusive mass transfer, potentially locking or unlocking slip (Angevine et al., 1982). The influence of rate and state friction can also produce pulses of alternating slip rate due to changes in the smoothing factor (see Biemiller and Lavier, 2017, their Fig. 4e). We suggest that these complex changes in fault zone rheology may influence how slip is distributed within the anastomosing network of faults that includes the Pisia and Skinos Faults.

Another scenario may be that, although a single relatively narrow shear zone ~1–2 km wide is likely to exist at depth beneath the brittle-viscous transition under the Pisia and Skinos Faults, perhaps at times different portions of this shear zone are at different stages of the dislocation creep and annealing cycle. Dislocations piling up at grain boundaries in one portion of the shear zone could promote strain-hardening, whilst elsewhere within the same shear zone annealing could produce new strain-free grains that promote renewed dislocation creep (Knipe, 1989; compare with Dolan et al., 2007); this may activate either the Pisia Fault or Skinos Fault at any one time. At other times the rheology of the shear-zone might be uniform across its extent promoting simultaneous slip on both the Pisia and Skinos faults.

Whatever the cause of the alternating slip behaviour on the 10^3–10^4 years timescale, in the case of the Skinos and Pisia Faults, shared growth is implied by the fact that both faults have slipped by similar amounts over several million years evidenced by the similar ~450 m offsets of features in the pre-rift geology such as the thrust carrying the ophiolite (Figs. 1e and 7b). The faults also share the same post slope stabilisation slip of 14.6 m which has developed over the last few tens of millennia (Fig. 3aiii, biii and Fig. 7c; Electronic Supplement S2af and S2bf). On the coseismic timescale of a single earthquake sequence, shared fault growth has been evidenced by the spatially out-of-phase throw profiles from the 1981 earthquakes, where slip deficits in the set of ruptures from one fault seem to be filled in by slip maxima in the set of ruptures from the other fault, immediately across-strike, and vice versa (Figs. 1f and 7e)

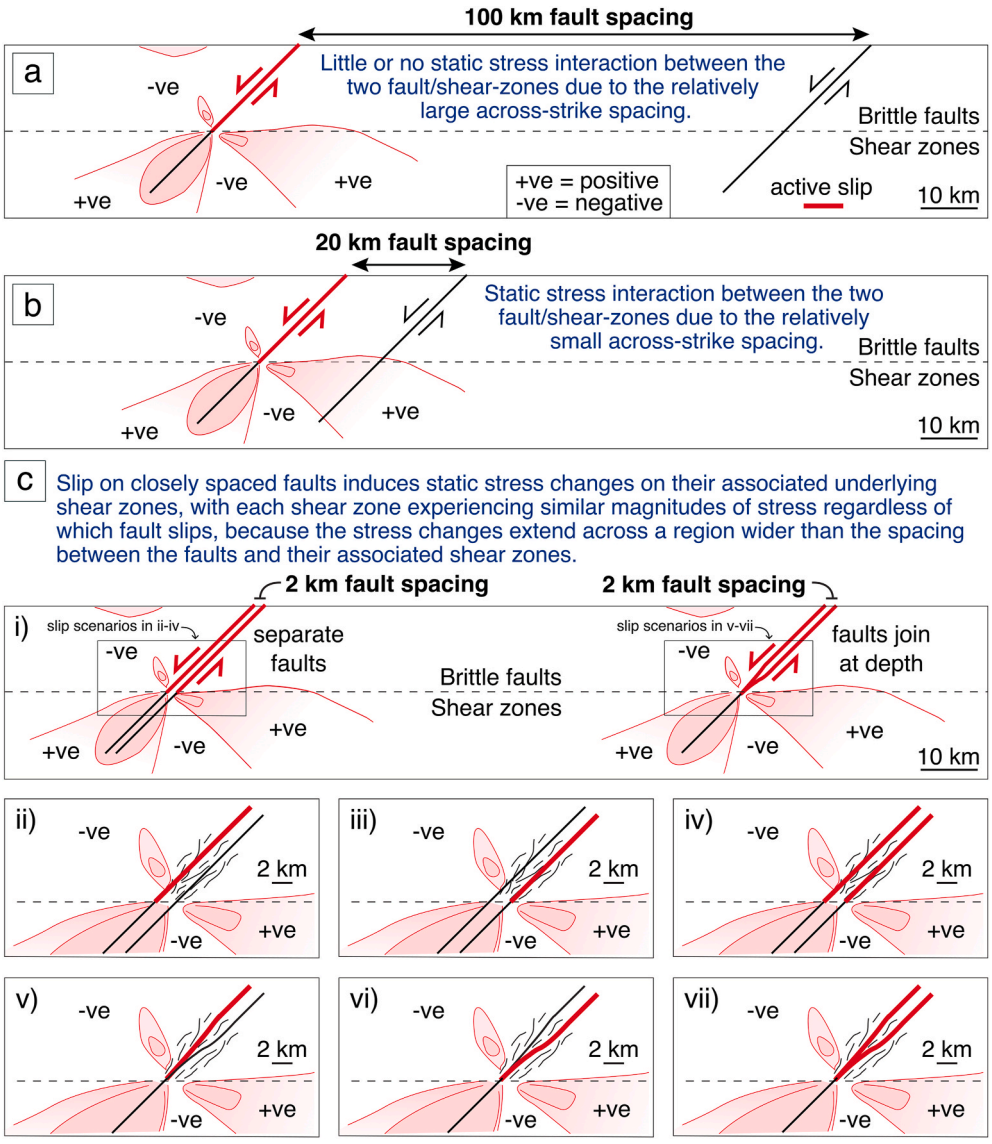

Fig. 8. Three scenarios for the spacing between fault/shear-zone structures with stress contours for positive differential stress changes produced by coseismic slip (slipping faults marked by a thick red line) on one of the faults (differential stress contours redrawn from Mildon et al., 2022, their Fig. 2). All three fault spacings have been shown to exhibit out-of-phase fault behaviour (adapted from ideas in Dolan et al., 2007; Mildon et al., 2022; Roberts et al., 2024; this study). (a) 100 km spacing is too large for stress interactions to explain out-of-phase behaviour, which may instead be produced by competing rates of rapid viscous slip, strain hardening and annealing, with the weakest shear zone at any given time localising coseismic slip above it (Dolan et al., 2007). (b) 20 km spacing allows stress interactions to change viscous strain rates on shear zones because strain rate is proportional to the differential stress raised to the power "n" (Hirth et al., 2001), and this has been shown to be consistent with out-of-phase behaviour for this fault spacing (Mildon et al., 2022; Roberts et al., 2024). (c) 2 km fault spacing (this study) implies that the viscous roots of both faults will share similar stress histories because of their close spacing, and hence may also share similar microstructural evolution. The reason for the out-of-phase and simultaneous slip behaviour documented in this study is unclear, yet fault spacings as low as 2 km are common worldwide, so this requires further study. (i) Possible arrangements of closely spaced faults at depth, either separated or joined. The stress patterns are schematic and not re-calculated for the exact slip distribution as we only seek to show the relative across-strike length scales of the fault spacing and stress changes. (ii), (iii) and (iv) are slip scenarios for separated faults, and (v), (vi) and (vii) are slip scenarios for joined faults located in the left and right boxes of (i), respectively. (ii) to (vii) show how slip can take alternative routes through a mesh of closely spaced faults and thus share similar overall imposed stresses. (For interpretation of the references to colour in this figure legend, the reader is referred to the Web version of this article.)

(Mitchell et al., 2024). Thus, over timescales of a few seconds to hours during single earthquake sequences, over timescales of a few tens of millennia since slope stabilisation, and over timescales of a few million years associated with offsets or pre-existing thrusts, neither fault seems to dominate slip. Combining this evidence, we suggest that the two faults may, in general, share slip through being connected at depth by a shared shear zone and an anastomosing network of faults. In other words, the Skinos and Pisia Faults appear to be acting as a single combined fault-zone/shear-zone.

These complexities in the temporal and spatial patterns of slip over different timescales are important because other examples of normal faults with similar structural geometries exist worldwide, and they may show similar complexity in behaviour. For example, in the Basin and Range Province of the US, the Pleasant Valley Fault (Wallace et al., 1984), Hebgen Lake Fault (Doser, 1985) and Dixie Valley and Fairview Peak Faults (Slemmons, 1957; Scholz, 2010) all experienced historical earthquake rupture of across-strike faults spaced by distances of just a few kilometres, similar to that for the Skinos and Pisia Faults. We have discussed possible reasons for the complexity of slip over different time periods, but clearly further work is required to constrain the reasons for

out-of-phase and simultaneous slip on faults that are so closely spaced across strike that they are likely to share the same underlying shear zone. In particular, such research could help better understand the probability of across-strike faults co-rupturing and help identify the fault configurations that could either increase or decrease the likelihood of subsequent earthquake ruptures occurring on closely spaced across-strike faults.

Multi-fault ruptures, as implied by our hypothesised mechanism(s) and identification of simultaneous slip on both faults, may suggest that the faults could rupture individually or both rupture together. The latter would likely produce a higher magnitude of earthquake shaking. In addition, in terms of determining the nature of segment boundaries for the assessment of seismic hazard, it has been suggested that some segment boundaries may either be persistent, meaning they always stop the migration of ruptures, or non-persistent, meaning they sometimes allow ruptures to jump across them (Wheeler et al., 1989; Crone and Haller, 1991; Zhang et al., 1991; DuRoss, 2008; DuRoss et al., 2016; Philibosian and Meltzner, 2020). For example, one estimate suggests that a segment boundary of 3–4 km across will be persistent, with examples with smaller dimensions being non-persistent (Wesnousky, 2006). Indeed, it has since been proposed that specific size parameters, such as these dimensions of fault segment boundaries, determine whether ruptures can jump from one fault across a segment boundary onto a neighbouring fault (Field et al., 2009, 2014). However, for the Pisia and Skinos Faults, our findings indicate that at times ruptures can jump between the two faults, separated in time by just a few hours, whilst at other times they do not, indicating that the structure can alternate between being persistent or non-persistent.

Another critical factor highlighted by our work that should be considered for the assessment of seismic hazard, is that while the regional extension rate is probably constant through time, it is likely to be partitioned differently between individual structures through time (e.g. Jackson, 1987). This is evidenced by our finding that slip rates fluctuate over multi-millennial timescales. For example, using inferred average slip rates for the Skinos Fault (0.25 mm/yr, 2.5 mm/yr, and 1.38 mm/yr) and the Pisia Fault (1.25 mm/yr, 0.25 mm/yr, and 1.38 mm/yr) across time slices of 10–6 ka, 6–2 ka, and 2–0 ka, and applying fault dips of 59° and 62°, respectively, we calculated combined heave rates of 0.72 mm/yr (10–6 ka), 1.40 mm/yr (6–2 ka), and 1.35 mm/yr (2–0 ka). These results reveal significant temporal variability in heave rate, and thus extension rates, with the combined rate nearly doubling from 0.72 mm/yr (10–6 ka) to 1.40 mm/yr (6–2 ka), before a slight decrease to 1.35 mm/yr in the most recent time slice. We argue that these heave-rate changes reflect changes in local strain accumulation and shifts in activity between faults. These combined heave rates are significantly lower than the GNSS-derived extension rate of 5–6 mm/yr for the eastern Gulf of Corinth (Briole et al., 2021), indicating that the Pisia and Skinos Faults alone cannot account for the full extension measured by GNSS, implying that multiple other active faults, probably offshore, contribute to the total strain budget of this region. However, our findings of slip rates varying through time suggests that faults in seismically active regions likely experience temporal changes in slip rates. These findings underscore the importance of incorporating temporal variability in local extension rates into probabilistic seismic hazard models to better capture the seismic hazard posed by fault systems with complex, time-dependent behaviour.

Overall, our work provides new insights into the seismic hazard represented by closely-spaced *en echelon* faults and highlights the need for further studies of earthquake recurrence on such structures over multi-millennial timescales.

6. Conclusions

This study analysed the multi-millennia slip rate histories of the closely spaced Skinos and Pisia Faults in Greece using *in situ* ^{36}Cl cosmogenic exposure dating. Our findings reveal a relationship of alternating out-of-phase slip and simultaneous slip, indicating interaction between these faults over millennial timescales.

(1) The Pisia Fault exhibited variable slip rates, with an initial low slip rate of ~0.5–0.75 mm/yr from ~20 ka to 9.6 ± 0.5 ka, followed by an increase to ~1.25 mm/yr until 5.2 ± 0.5 ka. After a subsequent decrease to ~0.25 mm/yr or less until ~2.0 ± 0.5 ka, its slip rate accelerated again to ~1.25–1.5 mm/yr to the present day.
(2) The Skinos Fault maintained a low slip rate of ~0.25 mm/yr or less until ~6.4 ± 0.5 ka, after which it accelerated to ~2.0–3.0 mm/yr, a rate that persisted until the present or slightly earlier, ~1 ka.
(3) Comparison of these slip histories reveals alternating periods of out-of-phase and simultaneous slip. Out-of-phase behaviour was observed between ~9.6 ka and ~6.4 ka, as well as from ~5.2 ka to ~2.0 ka, and simultaneous slip occurred from ~6.4 ka to ~5.2 ka and from ~2.0 ka to the present or ~1 ka. This pattern may suggest that the faults interact through a shared underlying shear zone and are connected by a network of faults above the brittle-ductile transition. The slip on the faults may be dictated by changes in frictional resistance within the fault gouge in the network of faults.
(4) These findings have broader implications for fault systems globally, as similar interactions may occur in other regions with closely spaced across-strike faults. Further studies integrating ^{36}Cl cosmogenic dating are needed to identify slip relationships over millennial timescales.
(5) These findings contribute to seismic hazard assessment by demonstrating that slip may be shared between across-strike faults within the evolving South Alkyonides Fault Zone. Future research should investigate how fault rheology and stress interactions influence rupture propagation and earthquake clustering, ultimately refining models of fault behaviour and seismic risk.

We recommend similar studies of fault behaviour over different timescales should be conducted on other examples of closely spaced across-strike faults. Analysing slip relationships between across-strike faults using fault slip histories over multi-millennia, as demonstrated herein, may prove crucial for understanding earthquake activity, the faulting process and the potential seismic hazard associated with such complex fault systems.

CRediT authorship contribution statement

Sam Mitchell: Writing – review & editing, Writing – original draft, Methodology, Investigation, Funding acquisition, Formal analysis, Conceptualization. **Claudia Sgambato:** Writing – review & editing, Methodology, Investigation, Formal analysis, Conceptualization. **Jenni Robertson:** Writing – review & editing, Methodology, Investigation, Formal analysis, Conceptualization. **Gerald P. Roberts:** Writing – review & editing, Supervision, Methodology, Investigation, Funding acquisition, Formal analysis, Conceptualization. **Joanna P. Faure Walker:** Writing – review & editing, Supervision, Methodology, Investigation, Funding acquisition, Formal analysis, Conceptualization. **Zoë Mildon:** Writing – review & editing, Funding acquisition, Conceptualization. **Athanassios Ganas:** Writing – review & editing. **Ioannis Papanikolaou:** Writing – review & editing. **Francesco Iezzi:** Writing – review & editing. **Joakim Beck:** Writing – review & editing, Methodology. **Steven A. Binnie:** Writing – review & editing, Investigation. **Tibor Dunai:** Writing – review & editing, Investigation. **Damián A. López:** Writing – review & editing, Investigation. **Georgios Deligiannakis:** Writing – review & editing. **Silke Mechernich:** Writing – review & editing. **Klaus Reicherter:** Writing – review & editing. **Elias J. Rugen:** Writing – review & editing, Investigation.

Declaration of competing interest

The authors declare that they have no known competing financial interests or personal relationships that could have appeared to influence the work reported in this paper.

Acknowledgements

This work was supported by the Natural Environment Research Council with a studentship awarded to Sam Mitchell [grant number NE/S007229/1] and grant to Prof. Gerald Roberts, Prof. Joanna Faure Walker, and Dr. Zoë Mildon [grant number NE/VO12894/1]. We thank Manuel Curzi and an anonymous reviewer for helping to improve the manuscript.

Appendix A. Supplementary data

Supplementary data to this article can be found online at https://doi.org/10.1016/j.jsg.2025.105445.

Data availability

The data used for this study are available in the supplementary material accompanying the article.

References

Abercrombie, R.E., Main, I.G., Douglas, A., Burton, P.W., 1995. The nucleation and rupture process of the 1981 Gulf of Corinth earthquakes from deconvolved broad-band data. Geophys. J. Int. 120, 393–405.
Allen, J.R., Brandt, U., Brauer, A., Hubberten, H.W., Huntley, B., Keller, J., Kraml, M., Mackensen, A., Mingram, J., Negendank, J.F., Nowaczyk, N.R., 1999. Rapid environmental changes in southern Europe during the last glacial period. Nature 400, 740–743.
Ambraseys, N.N., Jackson, J.A., 1990. Seismicity and associated strain of central Greece between 1890 and 1988. Geophys. J. Int. 101, 663–708.
Angevine, C.L., Turcotte, D.L., Furnish, M.D., 1982. Pressure solution lithification as a mechanism for the stick-slip behavior of faults. Tectonics 1, 151–160.
Armijo, R., Meyer, B.G.C.P., King, G.C.P., Rigo, A., Papanastassiou, D., 1996. Quaternary evolution of the Corinth Rift and its implications for the late cenozoic evolution of the aegean. Geophys. J. Int. 126, 11–53.
Beck, J., Wolfers, S., Roberts, G.P., 2018. Bayesian earthquake dating and seismic hazard assessment using chlorine-36 measurements (BED v1). Geosci. Model Dev. (GMD) 11, 4383–4397.
Bell, R.E., McNeill, L.C., Bull, J.M., Henstock, T.J., Collier, R.L., Leeder, M.R., 2009. Fault architecture, basin structure and evolution of the Gulf of Corinth Rift, central Greece. Basin Res. 21, 824–855.
Benedetti, L., Finkel, R., King, G., Armijo, R., Papanastassiou, D., Ryerson, F.J., Flerit, F., Farber, D., Stavrakakis, G., 2003. Motion on the Kaparelli fault (Greece) prior to the 1981 earthquake sequence determined from 36Cl cosmogenic dating. Terra Nova 15, 118–124.
Benedetti, L., Finkel, R., Papanastassiou, D., King, G., Armijo, R., Ryerson, F., Farber, D., Flerit, F., 2002. Post-glacial slip history of the Sparta fault (Greece) determined by 36Cl cosmogenic dating: evidence for non-periodic earthquakes. Geophys. Res. Lett. 29, 87-1.
Benedetti, L., Manighetti, I., Gaudemer, Y., Finkel, R., Malavieille, J., Pou, K., Arnold, M., Aumaître, G., Bourlès, D., Keddadouche, K., 2013. Earthquake synchrony and clustering on Fucino faults (Central Italy) as revealed from in situ 36Cl exposure dating. J. Geophys. Res. Solid Earth 118, 4948–4974.
Biemiller, J., Lavier, L., 2017. Earthquake supercycles as part of a spectrum of normal fault slip styles. J. Geophys. Res. Solid Earth 122, 3221–3240.
Billiris, H., Paradissis, D., Veis, G., England, P., Featherstone, W., Parsons, B., Cross, P., Rands, P., Rayson, M., Sellers, P., Ashkenazi, V., Davison, M., Jackson, J., Ambraseys, N., 1991. Geodetic determination of tectonic deformation in central Greece from 1900 to 1988. Nature 350, 124–129.
Bornovas, I., Eleftheriou, A., Gaitanakis, P., 1984a. Geological Map of Greece, 1:50.000 Scale Kaparellion Sheet. Institute of Geology and Mineral Exploration (IGME), Athens.
Bornovas, I., Gaitanakis, P., Spiridopoulos, A., 1984b. Geological Map of Greece, 1:50 000 Scale, Perachora Sheet. Institute of Geology and Mineral Exploration (IGME), Athens.
Briole, P., Ganas, A., Elias, P., Dimitrov, D., 2021. The GPS velocity field of the Aegean. New observations, contribution of the earthquakes, crustal blocks model. Geophys. J. Int. 226, 468–492.
Cladouhos, T.T., 1999. Shape preferred orientations of survivor grains in fault gouge. J. Struct. Geol. 21, 419–436.
Clarke, P.J., Davies, R.R., England, P.C., Parsons, B., Billiris, H., Paradissis, D., Veis, G., Cross, P.A., Denys, P.H., Ashkenazi, V., 1998. Crustal strain in central Greece from repeated GPS measurements in the interval 1989-1997. Geophys. J. Int. 135, 195–214.
Collier, R.E.L., Pantosti, D., D'Addezio, G., De Martini, P.M., Masana, E., Sakellariou, D., 1998. Paleoseismicity of the 1981 Corinth earthquake fault: seismic contribution to extensional strain in central Greece and implications for seismic hazard. J. Geophys. Res. Solid Earth 103, 30001–30019.
Cowie, P.A., Phillips, R.J., Roberts, G.P., McCaffrey, K., Zijerveld, L.J.J., Gregory, L.C., Faure Walker, J.P., Wedmore, L.N.J., Dunai, T.J., Binnie, S.A., Freeman, S.P.H.T., 2017. Orogen-scale uplift in the central Italian Apennines drives episodic behaviour of earthquake faults. Sci. Rep. 7, 44858.
Cowie, P.A., Scholz, C.H., Roberts, G.P., Faure Walker, J.P., Steer, P., 2013. Viscous roots of active seismogenic faults revealed by geologic slip rate variations. Nat. Geosci. 6, 1036–1040.
Crone, A.J., Haller, K.M., 1991. Segmentation and the coseismic behavior of Basin and Range normal faults: examples from east-central Idaho and southwestern Montana, USA. J. Struct. Geol. 13, 151–164.
Curzi, M., Bernasconi, S.M., Billi, A., Boschi, C., Aldega, L., Franchini, S., Albert, R., Gerdes, A., Barberio, M.D., Looser, N., Carminati, E., 2021. U-Pb age of the 2016 Amatrice earthquake causative fault (Mt. Gorzano, Italy) and paleo-fluid circulation during seismic cycles inferred from inter-and co-seismic calcite. Tectonophysics 819, 229076.
Davis Jr., R., Schaeffer, O.A., 1955. Chlorine-36 in nature. Ann. N. Y. Acad. Sci. 62, 107–121.
Di Toro, G., Han, R., Hirose, T., De Paola, N., Nielsen, S., Mizoguchi, K., Ferri, F., Cocco, M., Shimamoto, T., 2011. Fault lubrication during earthquakes. Nature 471, 494–498.
Dolan, J.F., Bowman, D.D., Sammis, C.G., 2007. Long-range and long-term fault interactions in Southern California. Geology 35, 855–858.
Dolan, J.F., McAuliffe, L.J., Rhodes, E.J., McGill, S.F., Zinke, R., 2016. Extreme multi-millennial slip rate variations on the Garlock fault, California: strain super-cycles, potentially time-variable fault strength, and implications for system-level earthquake occurrence. Earth Planet Sci. Lett. 446, 123–136.
Dolan, J.F., Meade, B.J., 2017. A comparison of geodetic and geologic rates prior to large strike-slip earthquakes: a diversity of earthquake-cycle behaviors? G-cubed 18, 4426–4436.
Dolan, J.F., Van Dissen, R.J., Rhodes, E.J., Zinke, R., Hatem, A.E., McGuire, C., Langridge, R.M., Grenader, J.R., 2024. One tune, many tempos: faults trade off slip in time and space to accommodate relative plate motions. Earth Planet Sci. Lett. 625, 118484.
Doser, D.I., 1985. Source parameters and faulting processes of the 1959 Hebgen Lake, Montana, earthquake sequence. J. Geophys. Res. Solid Earth 90, 4537–4555.
Dunai, T.J., 2010. Cosmogenic Nuclides: Principles, Concepts and Applications in the Earth Surface Sciences. Cambridge University Press.
Dunai, T.J., 2000. Scaling factors for production rates of in situ produced cosmogenic nuclides: a critical reevaluation. Earth Planet Sci. Lett. 176, 157–169.
DuRoss, C.B., 2008. Holocene vertical displacement on the central segments of the Wasatch fault zone, Utah. Bull. Seismol. Soc. Am. 98, 2918–2933.
DuRoss, C.B., Personius, S.F., Crone, A.J., Olig, S.S., Hylland, M.D., Lund, W.R., Schwartz, D.P., 2016. Fault segmentation: new concepts from the Wasatch fault zone, Utah, USA. J. Geophys. Res. Solid Earth 121, 1131–1157.
Evelpidou, N., Ganas, A., Karkani, A., Spyrou, E., Saitis, G., 2023. Late quaternary relative sea-level changes and vertical GNSS motions in the gulf of Corinth: the asymmetric localization of deformation inside an active half-graben. Geosciences 13, 329.
Fairbanks, R.G., 1989. A 17,000-year glacio-eustatic sea level record: influence of glacial melting rates on the Younger Dryas event and deep-ocean circulation. Nature 342, 637–642.
Field, E.H., Arrowsmith, R.J., Biasi, G.P., Bird, P., Dawson, T.E., Felzer, K.R., Jackson, D. D., Johnson, K.M., Jordan, T.H., Madden, C., Michael, A.J., 2014. Uniform California earthquake rupture forecast, version 3 (UCERF3)—the time-independent model. Bull. Seismol. Soc. Am. 104, 1122–1180.
Field, E.H., Dawson, T.E., Felzer, K.R., Frankel, A.D., Gupta, V., Jordan, T.H., Parsons, T., Petersen, M.D., Stein, R.S., Weldon, R.J., Wills, C.J., 2009. Uniform California earthquake rupture forecast, version 2 (UCERF 2). Bull. Seismol. Soc. Am. 99, 2053–2107.
Ford, M., Rohais, S., Williams, E.A., Bourlange, S., Jousselin, D., Backert, N., Malartre, F., 2013. Tectono-sedimentary evolution of the western Corinth rift (Central Greece). Basin Res. 25, 3–25.
Fossen, H., Cavalcante, G.C.G., 2017. Shear zones–A review. Earth Sci. Rev. 171, 434–455.
Galli, P., Galadini, F., Pantosti, D., 2008. Twenty years of paleoseismology in Italy. Earth Sci. Rev. 88, 89–117.
Galli, P., Galderisi, A., Messina, P., Peronace, E., 2022. The Gran Sasso fault system: paleoseismological constraints on the catastrophic 1349 earthquake in Central Italy. Tectonophysics 822, 229156.
Ganas, A., Oikonomou, A., Tsimi, C., 2013. Noafaults: a digital database for active faults in Greece. National Documentation Centre 47, 518–530.
Ganas, A., Sokos, E., Agalos, A., Leontakianakos, G., Pavlides, S., 2006. Coulomb stress triggering of earthquakes along the Atalanti Fault, central Greece: two April 1894 M6+ events and stress change patterns. Tectonophysics 420, 357–369.
Gawthorpe, R.L., Fabregas, N., Pechlivanidou, S., Ford, M., Collier, R.E.L., Carter, G.D., McNeill, L.C., Shillington, D.J., 2022. Late Quaternary mud-dominated, basin-floor sedimentation of the Gulf of Corinth, Greece: implications for deep-water depositional processes and controls on syn-rift sedimentation. Basin Res. 34, 1567–1600.

Gawthorpe, R.L., Leeder, M.R., Kranis, H., Skourtsos, E., Andrews, J.E., Henstra, G.A., Mack, G.H., Muravchik, M., Turner, J.A., Stamatakis, M., 2018. Tectono-sedimentary evolution of the plio-pleistocene Corinth rift, Greece. Basin Res. 30, 448–479.
Giraudi, C., Frezzotti, M., 1986. Inversione pleistocenica del drenaggio in alta Val Roveto (Abruzzes sud-occidentale). Mem. Soc. Geol. It. 35, 847–853.
Giraudi, C., Frezzotti, M., 1997. Late Pleistocene glacial events in the central Apennines, Italy. Quaternary research 48, 280–290.
Goldsworthy, M., Jackson, J., 2000. Active normal fault evolution in Greece revealed by geomorphology and drainage patterns. J. Geol. Soc. 157, 967–981.
Goldsworthy, M., Jackson, J., Haines, J., 2002. The continuity of active fault systems in Greece. Geophys. J. Int. 148, 596–618.
Gosse, J.C., Phillips, F.M., 2001. Terrestrial in situ cosmogenic nuclides: theory and application. Quat. Sci. Rev. 20, 1475–1560.
Guidoboni, E., Traina, G., Comastri, A., 1994. Catalogue of Ancient Earthquakes in the Mediterranean Sea up to the 10th Century.
Hirth, G., Teyssier, C., Dunlap, J.W., 2001. An evaluation of quartzite flow laws based on comparisons between experimentally and naturally deformed rocks. Int. J. Earth Sci. 90, 77–87.
Hubert, A., King, G., Armijo, R., Meyer, B., Papanastasiou, D., 1996. Fault re-activation, stress interaction and rupture propagation of the 1981 Corinth earthquake sequence. Earth Planet Sci. Lett. 142, 573–585.
Iezzi, F., Roberts, G.P., Faure Walker, J.P., Papanikolaou, I., Ganas, A., Deligiannakis, G., Beck, J., Wolfers, S., Gheorghiu, D., 2021. Temporal and spatial earthquake clustering revealed through comparison of millennial strain rates from 36Cl cosmogenic exposure dating and decadal GPS strain rate. Sci. Rep. 11, 23320.
Jackson, J., 1987. Active Normal Faulting and Crustal Extension, vol. 28. Geological Society, London, Special Publications, pp. 3–17.
Jackson, J., 1994. Active tectonics of the Aegean region. Annu. Rev. Earth Planet Sci. 22, 239–271.
Jackson, J., Gagnepain, J., Houseman, G.A., King, G.C., Papadimitriou, P., Soufleris, C., Virieux, J.V., 1982. Seismicity, normal faulting, and the geomorphological development of the gulf of Corinth (Greece): the Corinth earthquakes of february and March 1981. Earth Planet Sci. Lett. 57, 377–397.
Jolivet, L., 2001. A comparison of geodetic and finite strain pattern in the Aegean, geodynamic implications. Earth Planet Sci. Lett. 187, 95–104.
Jolivet, L., Daniel, J.M., Truffert, C., Goffé, B., 1994. Exhumation of deep crustal metamorphic rocks and crustal extension in arc and back-arc regions. Lithos 33, 3–30.
Jolivet, L., Faccenna, C., Huet, B., Labrousse, L., Le Pourhiet, L., Lacombe, O., Lecomte, E., Burov, E., Denèle, Y., Brun, J.-P., Philippon, M., Paul, A., Salaün, G., Karabulut, H., Piromallo, C., Monié, P., Gueydan, F., Okay, A.I., Oberhänsli, R., Pourteau, A., Augier, R., Gadenne, L., Driussi, O., 2013. Aegean tectonics: strain localisation, slab tearing and trench retreat. Tectonophysics 597–598, 1–33.
Kelletat, D., Kowalczyk, G., Schröder, B., Winter, K.-P., 1976. A synoptic view on the neotectonic development of the peloponnesian coastal regions. Z. Dtsch. Geol. Ges. 127, 447–465.
Knipe, R.J., 1989. Deformation mechanisms—recognition from natural tectonites. J. Struct. Geol. 11, 127–146.
Lal, D., 1991. Cosmic ray labeling of erosion surfaces: in situ nuclide production rates and erosion models. Earth Planet Sci. Lett. 104, 424–439.
Le Pichon, X., Angelier, J., 1979. The Hellenic arc and trench system: a key to the neotectonic evolution of the eastern Mediterranean area. Tectonophysics 60, 1–42.
Le Pichon, X., Chamot-Rooke, N., Lallemant, S., Noomen, R., Veis, G., 1995. Geodetic determination of the kinematics of central Greece with respect to Europe: implications for eastern Mediterranean tectonics. J. Geophys. Res. Solid Earth 100, 12675–12690.
Leeder, M.R., Portman, C., Andrews, J.E., Collier, R.L., Finch, E., Gawthorpe, R.L., McNeill, L.C., Perez-Arlucea, M., Rowe, P., 2005. Normal faulting and crustal deformation, Alkyonides Gulf and Perachora peninsula, eastern Gulf of Corinth rift, Greece. J. Geol. Soc. 162, 549–561.
Leeder, M.R., Seger, M.J., Stark, C.P., 1991. Sedimentation and tectonic geomorphology adjacent to major active and inactive normal faults, southern Greece. J. Geol. Soc. 148, 331–343.
McKenzie, D., 1972. Active tectonics of the Mediterranean region. Geophys. J. Int. 30, 109–185.
Mechernich, S., Reicherter, K., Deligiannakis, G., Papanikolaou, I., 2023. Tectonic geomorphology of active faults in Eastern Crete (Greece) with slip rates and earthquake history from cosmogenic 36Cl dating of the Lastros and Orno faults. Quat. Int. 651, 77–91.
Mechernich, S., Schneiderwind, S., Mason, J., Papanikolaou, I.D., Deligiannakis, G., Pallikarakis, A., Binnie, S.A., Dunai, T.J., Reicherter, K., 2018. The seismic history of the Pisia fault (eastern Corinth rift, Greece) from fault plane weathering features and cosmogenic 36Cl dating. J. Geophys. Res. Solid Earth 123, 4266–4284.
Mildon, Z.K., Roberts, G.P., Faure Walker, J.P., Beck, J., Papanikolaou, I., Michetti, A.M., Toda, S., Iezzi, F., Campbell, L., McCaffrey, K.J., Shanks, R., 2022. Surface faulting earthquake clustering controlled by fault and shear-zone interactions. Nat. Commun. 13, 7126.
Mitchell, S., Roberts, G.P., Faure Walker, J.P., Iezzi, F., Sgambato, C., Robertson, J., Mildon, Z.K., Ganas, A., Papanikolaou, I.D., Rugen, E.J., 2024. The relationship between kinematics and fault geometry for surface coseismic ruptures on across-strike faults: new observations of slip vectors and displacements along the Pisia and Skinos faults from the 1981 Eastern Gulf of Corinth, Greece earthquakes. J. Struct. Geol. 182, 105117.
Morewood, N.C., Roberts, G.P., 1997. Geometry, kinematics and rates of deformation in a normal fault segment boundary, central Greece. Geophys. Res. Lett. 24, 3081–3084.
Morewood, N.C., Roberts, G.P., 1999. Lateral propagation of the surface trace of the South Alkyonides normal fault segment, central Greece: its impact on models of fault growth and displacement–length relationships. J. Struct. Geol. 21, 635–652.
Morewood, N.C., Roberts, G.P., 2001. Comparison of surface slip and focal mechanism slip data along normal faults: an example from the eastern Gulf of Corinth, Greece. J. Struct. Geol. 23, 473–487.
Moore, J.D., Parsons, B., 2015. Scaling of viscous shear zones with depth-dependent viscosity and power-law stress–strain rate dependence. Geophys. J. Int. 202, 242–260.
Nixon, C.W., McNeill, L.C., Bull, J.M., Bell, R.E., Gawthorpe, R.L., Henstock, T.J., Christodoulou, D., Ford, M., Taylor, B., Sakellariou, D., Ferentinos, G., 2016. Rapid spatiotemporal variations in rift structure during development of the Corinth Rift, central Greece. Tectonics 35, 1225–1248.
Ohl, M., Nzogang, B., Mussi, A., Wallis, D., Drury, M., Plümper, O., 2021. Crystal-plastic deformation in seismically active carbonate fault rocks. J. Geophys. Res. Solid Earth 126.
Palumbo, L., Benedetti, L., Bourlès, D., Cinque, A., Finkel, R., 2004. Slip history of the Magnola fault (Apennines, Central Italy) from 36Cl surface exposure dating: evidence for strong earthquakes over the Holocene. Earth Planet Sci. Lett. 225, 163–176.
Papadopoulos, G.A., Ganas, A., Agalos, A., et al., 2017. Earthquake triggering inferred from rupture histories, DInSAR ground deformation and stress-transfer modelling: the case of Central Italy during august 2016–january 2017. Pure Appl. Geophys. 174.
Papanikolaou, D., 2009. Timing of tectonic emplacement of the ophiolites and terrane paleogeography in the Hellenides. Lithos 108, 262–280.
Papanikolaou, D., 2013. Tectonostratigraphic models of the Alpine terranes and subduction history of the Hellenides. Tectonophysics 595, 1–24.
Papanikolaou, I.D., Triantaphyllou, M., Pallikarakis, A., Migiros, G., 2015. Active faulting at the Corinth Canal based on surface observations, borehole data and paleoenvironmental interpretations. Passive rupture during the 1981 earthquake sequence? Geomorphology 237, 65–78.
Peckover, E.N., Andrews, J.E., Leeder, M.R., Rowe, P.J., Marca, A., Sahy, D., Noble, S., Gawthorpe, R., 2019. Coupled stalagmite–Alluvial fan response to the 8.2 ka event and early Holocene palaeoclimate change in Greece. Palaeogeogr. Palaeoclimatol. Palaeoecol. 532, 109252.
Piccardi, L., Gaudemer, Y., Tapponnier, P., Boccaletti, M., 1999. Active oblique extension in the central Apennines (Italy): evidence from the Fucino region. Geophys. J. Int. 139, 499–530.
Philibosian, B., Meltzner, A.J., 2020. Segmentation and supercycles: a catalog of earthquake rupture patterns from the Sumatran Sunda Megathrust and other well-studied faults worldwide. Quat. Sci. Rev. 241, 106390.
Pousse-Beltran, L., Benedetti, L., Fleury, J., Boncio, P., Guillou, V., Pace, B., Rizza, M., Puliti, I., Socquet, A., Aster Team, 2022. 36Cl exposure dating of glacial features to constrain the slip rate along the Mt. Vettore Fault (Central Apennines, Italy). Geomorphology 412, 108302.
Roberts, G.P., 1996. Noncharacteristic normal faulting surface ruptures from the Gulf of Corinth, Greece. J. Geophys. Res. Solid Earth 101, 25255–25267.
Roberts, G.P., Ganas, A., 2000. Fault-slip directions in central and southern Greece measured from striated and corrugated fault planes: comparison with focal mechanism and geodetic data. J. Geophys. Res. Solid Earth 105, 23443–23462.
Roberts, G.P., Gawthorpe, R., Stewart, I., 1993. Surface faulting within active normal fault zones: examples from the Gulf of Corinth fault system, Central Greece. Zeitschrift fur Geomorphologie 94, 303–328.
Roberts, G.P., Houghton, S.L., Underwood, C., Papanikolaou, I., Cowie, P.A., van Calsteren, P., Wigley, T., Cooper, F.J., McArthur, J.M., 2009. Localization of Quaternary slip rates in an active rift in 105 years: an example from central Greece constrained by 234U-230Th coral dates from uplifted paleoshorelines. J. Geophys. Res. Solid Earth 114.
Roberts, S., Jackson, J., 1991. Active Normal Faulting in Central Greece: an Overview, vol. 56. Geological Society, London, Special Publications, pp. 125–142.
Roberts, G.P., Michetti, A.M., 2004. Spatial and temporal variations in growth rates along active normal fault systems: an example from the Lazio–Abruzzo Apennines, central Italy. J. Struct. Geol. 26, 339–376.
Roberts, G.P., Sgambato, C., Mildon, Z.K., Iezzi, F., Beck, J., Robertson, J., Papanikolaou, I., Michetti, A.M., Walker, J.F., Meschis, M., Shanks, R., Phillips, R., McCaffrey, K.J.W., Vittori, E., Mitchell, S., 2024. Spatial migration of temporal earthquake clusters driven by the transfer of differential stress between neighbouring fault/shear-zone structures. J. Struct. Geol., 105096
Roberts, G.P., Iezzi, F., Sgambato, C., Robertson, J., Beck, J., Mildon, Z.K., Papanikolaou, I., Michetti, A.M., Faure Walker, J.P., Mitchell, S., Meschis, M., 2025. Characteristics and modelling of slip-rate variability and temporal earthquake clustering across a distributed network of active normal faults constrained by in situ 36Cl cosmogenic dating of fault scarp exhumation, central Italy. J. Struct. Geol., 105391
Rohais, S., Eschard, R., Ford, M., Guillocheau, F., Moretti, I., 2007. Stratigraphic architecture of the plio-pleistocene infill of the Corinth Rift: implications for its structural evolution. Tectonophysics 440, 5–28.
Sakellariou, D., Lykousis, V., Alexandri, S., Kaberi, H., Rousakis, G., Nomikou, P., Georgiou, P., Ballas, D., 2007. Faulting, seismic-stratigraphic architecture and late quaternary evolution of the gulf of Alkyonides basin–east gulf of Corinth, Central Greece. Basin Res. 19, 273–295.
Schlagenhauf, A., Gaudemer, Y., Benedetti, L., Manighetti, I., Palumbo, L., Schimmelpfennig, I., Finkel, R., Pou, K., 2010. Using in situ Chlorine-36 cosmonuclide to recover past earthquake histories on limestone normal fault scarps: a reappraisal of methodology and interpretations. Geophys. J. Int. 182, 36–72.

Schlagenhauf, A., Manighetti, I., Benedetti, L., Gaudemer, Y., Finkel, R., Malavieille, J., Pou, K., 2011. Earthquake supercycles in Central Italy, inferred from 36Cl exposure dating. Earth Planet Sci. Lett. 307, 487–500.
Scholz, C.H., 2010. Large earthquake triggering, clustering, and the synchronization of faults. Bull. Seismol. Soc. Am. 100, 901–909.
Sgambato, C., Roberts, G.P., Iezzi, F., Faure Walker, J.P., Beck, J., Mildon, Z.K., Michetti, A.M., Vittori, E., Robertson, J., Gheorghiu, D.M., Shanks, R.P., 2025. Millennial slip-rates variability of along-strike active faults in the Italian Southern Apennines revealed by cosmogenic ^{36}Cl dating of fault scarps. Tectonics 44.
Slemmons, D.B., 1957. Geological effects of the Dixie Valley-Fairview Peak, Nevada, earthquakes of december 16, 1954. Bull. Seism. Soc. Am. 47, 353–375.
Stewart, I.S., Hancock, P.L., 1991. Scales of structural heterogeneity within neotectonic normal fault zones in the Aegean region. J. Struct. Geol. 13, 191–204.
Stone, J.O., 2000. Air pressure and cosmogenic isotope production. J. Geophys. Res. Solid Earth 105, 23753–23759.
Stone, J.O., Evans, J.M., Fifield, L.K., Allan, G.L., Cresswell, R.G., 1998. Cosmogenic chlorine-36 production in calcite by muons. Geochem. Cosmochim. Acta 62, 433–454.
Stone, J.O., Allan, G.L., Fifield, L.K., Cresswell, R.G., 1996. Cosmogenic chlorine-36 from calcium spallation. Geochem. Cosmochim. Acta 60, 679–692.
Taylor, B., Weiss, J.R., Goodliffe, A.M., Sachpazi, M., Laigle, M., Hirn, A., 2011. The structures, stratigraphy and evolution of the Gulf of Corinth rift, Greece. Geophys. J. Int. 185, 1189–1219.
Taymaz, T., Jackson, J., McKenzie, D., 1991. Active tectonics of the north and central Aegean Sea. Geophys. J. Int. 106, 433–490.
Tesson, J., Benedetti, L., 2019. Seismic history from in situ 36Cl cosmogenic nuclide data on limestone fault scarps using Bayesian reversible jump Markov chain Monte Carlo. Quat. Geochronol. 52, 1–20.
Tesson, J., Pace, B., Benedetti, L., Visini, F., Delli Rocioli, M., Arnold, M., Aumaître, G., Bourlès, D.L., Keddadouche, K., 2016. Seismic slip history of the Pizzalto fault (central Apennines, Italy) using in situ-produced 36Cl cosmic ray exposure dating and rare earth element concentrations. J. Geophys. Res. Solid Earth 121, 1983–2003.
Tikhomirov, D., Amiri, N.M., Ivy-Ochs, S., Alfimov, V., Vockenhuber, C., Akçar, N., 2019. Fault Scarp Dating Tool-a MATLAB code for fault scarp dating using in-situ chlorine-36 supplemented with datasets of Yavansu and Kalafat faults. Data Brief 26, 104476.
Vassilakis, E., Royden, L., Papanikolaou, D., 2011. Kinematic links between subduction along the Hellenic trench and extension in the Gulf of Corinth, Greece: a multidisciplinary analysis. Earth Planet Sci. Lett. 303, 108–120.
Vita-Finzi, C., King, G.C.P., 1985. The seismicity, geomorphology and structural evolution of the Corinth area of Greece. Phil. Trans. Roy. Soc. Lond. Math. Phys. Sci. 314, 379–407.
Walker, R.T., Claisse, S., Telfer, M., Nissen, E., England, P., Bryant, C., Bailey, R., 2010. Preliminary estimate of Holocene slip rate on active normal faults bounding the southern coast of the Gulf of Evia, central Greece. Geosphere 6, 583–593.
Wallace, R.E., Bonilla, M.G., Villalobos, H.A., 1984. Faulting Related to the 1915 Earthquakes in Pleasant Valley, Nevada (No. 1274-AB). US Geological Survey.
Wells, D.L., Coppersmith, K.J., 1994. New empirical relationships among magnitude, rupture length, rupture width, rupture area, and surface displacement. Bull. Seismol. Soc. Am. 84, 974–1002.
Wesnousky, S.G., 2006. Predicting the endpoints of earthquake ruptures. Nature 444, 358–360.
Wesnousky, S.G., 2008. Displacement and geometrical characteristics of earthquake surface ruptures: issues and implications for seismic-hazard analysis and the process of earthquake rupture. Bull. Seismol. Soc. Am. 98, 1609–1632.
Westaway, R., 1991. Continental Extension on Sets of Parallel Faults: Observational Evidence and Theoretical Models, vol. 56. Geological Society, London, Special Publications, pp. 143–169.
Wheeler, R.L., Schwartz, D.P., Sibson, R.H., 1989. Persistent segment boundaries on Basin-Range normal faults. US Geol. Surv. Open-File Rept. 87-673, 432–444.
Whittaker, A.C., Walker, A.S., 2015. Geomorphic constraints on fault throw rates and linkage times: examples from the Northern Gulf of Evia, Greece. J. Geophys. Res.: Earth Surf. 120, 137–158.
Zhang, P., Slemmons, D.B., Mao, F., 1991. Geometric pattern, rupture termination and fault segmentation of the Dixie Valley—Pleasant Valley active normal fault system, Nevada, USA. J. Struct. Geol. 13, 165–176.
Zhu, W., Allison, K.L., Dunham, E.M., Yang, Y., 2020. Fault valving and pore pressure evolution in simulations of earthquake sequences and aseismic slip. Nat. Commun. 11, 4833.
Zreda, M., Noller, J.S., 1998. Ages of prehistoric earthquakes revealed by cosmogenic chlorine-36 in a bedrock fault scarp at Hebgen Lake. Science 282, 1097–1099.
Zreda, M.G., Phillips, F.M., Elmore, D., Kubik, P.W., Sharma, P., Dorn, R.I., 1991. Cosmogenic chlorine-36 production rates in terrestrial rocks. Earth Planet Sci. Lett. 105, 94–109.